Convergence in simulating global soil organic carbon by structurally different models after data assimilation

Feng Tao[1, 2*], Benjamin Z. Houlton[3], Yuanyuan Huang[4], Ying-Ping Wang[5], Stefano Manzoni[6], Bernhard Ahrens[7], Umakant Mishra[8, 9], Lifen Jiang[10], Xiaomeng Huang[2, *], Yiqi Luo[10]

[1]Department of Ecology and Evolutionary Biology, Cornell University, Ithaca, NY, USA

[2]Department of Earth System Science, Ministry of Education Key Laboratory for Earth System Modelling, Institute for Global Change Studies, Tsinghua University, Beijing, China

[3]Department of Ecology and Evolutionary Biology and Department of Global Development, Cornell University, Ithaca, NY, USA

[4]Key Laboratory of Ecosystem Network Observation and Modeling, Institute of Geographic Sciences and Natural Resources Research, Chinese Academy of Sciences, Beijing, China

[5]CSIRO Environment, Private Bag 10, Clayton South VIC 3169, Australia

[6]Department of Physical Geography and Bolin Centre for Climate Research, Stockholm University, Stockholm, Sweden

[7]Max Planck Institute for Biogeochemistry, Jena, Germany

[8]Computational Biology and Biophysics, Sandia National Laboratories, Livermore, CA, USA

[9]Joint BioEnergy Institute, Lawrence Berkeley National Laboratory, Emeryville, CA, USA

[10]School of Integrative Plant Science, Cornell University, Ithaca NY, USA

Correspondence to: Feng Tao, phx.tao@gmail.com, Xiaomeng Huang, hxm@tsinghua.edu.cn

Abstract:

The current generation of biogeochemical models produce large uncertainty in carbon-climate feedback projections. Structural differences in these models have been identified as a major source of inter-model uncertainties when simulating soil organic carbon (SOC) dynamics worldwide. However, parameterization could also play a role, particularly when common observational data are used to constrain model simulations. Here we demonstrate the critical role of observational data in reducing model-based uncertainty in global estimates of SOC. We applied the PROcess-guided deep learning and DAta-driven modeling (PRODA) approach to constrain both a microbial implicit model based on first-order kinetics (i.e., Community Land Model version 5, CLM5) and a microbial explicit model based on Michaelis-Menten kinetics (i.e., CarbOn cycle and Microbial PArtitioning Soil model, COMPAS) with >50,000 globally distributed SOC vertical profiles. Overall, the two constrained models predicted similar carbon transfer efficiency, baseline decomposition rate, and environmental effects on carbon fluxes. These converged model components contributed to similar SOC patterns simulated by the two structurally different biogeochemical models. Carbon input allocation and vertical transport were less constrained by SOC profile data and require other data sets to constrain. Moreover, after being constrained by SOC observations, the Michaelis constant in COMPAS tends to be much larger than its corresponding substrate concentration in SOC decomposition. Thus, the Michaelis-Menten kinetics in the COMPAS model can be approximated by multiplicative kinetics (i.e., first order with respect to both donor and received pool carbon) in these global scale simulations. Our results highlight the importance of observational data in informing model development and constraining model predictions.

1. Introduction

Soils store more carbon than the atmosphere and vegetation combined (Ciais et al. 2014, Jackson et al. 2017). A small change in soil carbon storage can significantly impact the atmospheric carbon dioxide concentration and the climate. Substantial research has been conducted to understand the factors that underly the formation of soil organic carbon (SOC) and its persistence. A conventional paradigm focuses on the balance between plant carbon input as the source of SOC and organic matter decomposition that mineralizes SOC with different recalcitrance as CO_2 back to the atmosphere (Schmidt et al. 2011). Recently, increasing evidence suggests that soil microorganisms are the key determinant in partitioning soil carbon into accumulation versus loss (Cotrufo et al. 2013, Cotrufo et al. 2015, Bradford et al. 2016, Tao et al. 2023b). These two paradigms are the conceptual foundation of two classes of process-based models used to simulate global SOC dynamics. Because these model classes have distinctive structures that reflect different underlying theories and assumptions on soil carbon dynamics, large uncertainties in the simulated SOC emerge among models. Diverging simulations of SOC storage and its spatial distributions across the globe hinder a better understanding of the soil carbon cycle and its feedback to climate change (Todd-Brown et al. 2013, Ciais et al. 2014, Luo et al. 2016).

In simulating soil carbon dynamics, state-of-the-art process-based models structurally differ in classifying soil carbon pools, quantifying SOC decomposition kinetics, and representing carbon transfer processes (Chandel et al. 2023). To represent the heterogeneity of SOC, soil carbon is separated into conceptual pools with different turnover rates that indicate their decomposability. For example, models derived from the Century model (Parton et al. 1987) differentiate substrates according to turnover times, with labile substrates that cycle rapidly (i.e., active SOC) and chemically or physically protected pools that cycle slowly (i.e., slow and passive SOC). Recently formulated process-based models, carbon

pools are defined as measurable entities that can be validated with field observations (Abramoff et al. 2022) – e.g., microbial biomass, dissolved organic carbon, and mineral-associated organic carbon.

In representing SOC decomposition, a theory dating back to the 1980s portends that organic matter decay in soils follows first-order kinetics: $\frac{dSOC}{dt} = -k \times SOC$, where the loss rate of SOC (i.e., k) is independent of its pool size (i.e., SOC) (Parton et al. 1988) and thus, the SOC storage changes over time is proportional to its pool size (Forney and Rothman 2012). With increasing evidence pointing to microorganisms as a key factor in soil carbon dynamics, a newer generation of models have explored the possibility of nonlinearity in SOC decomposition (Schimel and Weintraub 2003, Allison et al. 2010, Georgiou et al. 2017, Wang et al. 2021). Among various nonlinear structures, the Michaelis-Menten kinetics (i.e., $\frac{dSOC}{dt} = -v\frac{ENZ \times SOC}{K+SOC}$) consider the interplay between the substrate (i.e., SOC) and the extracellular enzymes (i.e., ENZ) that catalyze the decomposition of organic matter (Schimel and Weintraub 2003, Wilson and Gerber 2021). Specifically, parameter v specifies the maximum SOC decomposition rate at its saturated content for a given enzyme content. The inverse of the Michaelis-Menten constant (K) specifies the enzyme's affinity for its substrate in a catalyzed reaction.

Process-based models also differ in allocating the decomposed carbon to other carbon pools or heterotrophic respiration as CO_2. While soil microbes mineralize SOC into CO_2 through their metabolism, transfers of decomposed carbon from one pool to another could result from either an exclusive effect of microbial processes or an integrative effect of biological, chemical, and physical reactions (i.e., including both microbial and non-microbial transfer). Specifically, when a model explicitly defines a microbial biomass carbon pool, , carbon received by this pool is partitioned according to microbial carbon use efficiency

(CUE) – i.e., the ratio of carbon assimilated in new biomass over carbon transferred from the substrate (Geyer et al. 2016, Manzoni et al. 2018, Tao et al. 2023b). Correspondingly, carbon transfers among compartments that happen without microbial carbon assimilation can be interpreted as results from other biochemical processes (e.g., microbial exudation and mortality) or organo-mineral interactions (Tao et al. 2023b). In contrast, for models without explicit representation of microbial biomass and assimilation processes, carbon transfer implicitly integrates the effects of both microbial physiology and other chemical or physical reactions. Depending on the model structure, a range of relations between long-term SOC and microbial traits such as CUE or carbon inputs to soil emerge (Wutzler and Reichstein 2008, Georgiou et al. 2017, He et al. 2023).

In addition to structural differences among varieties of process-based models, parameter values that quantify the strength and represent properties of different processes in the soil carbon cycle also contribute to the uncertainty of model simulations (Luo and Schuur 2020). Most current Earth system models adopt the Century-type model structure using first-order SOC decomposition kinetics. Notwithstanding their structural similarity, varying parameterizations among different models contribute to the divergent estimates of SOC storage both at the site-level and across the globe (Todd-Brown et al. 2013, Luo et al. 2015). Moreover, the same model with different parameterizations could also generate varying patterns of SOC and key model components, such as microbial CUE (Tao et al. 2023b) and plant carbon input (Tao et al. 2023a). However, parameterization and model structure are not fully independent in affecting model simulation: different model structures can in some cases converge to similar results in the long term via parameter adjustments. For example, the Michaelis-Menten kinetics, when the affinity of the enzyme for its substrate is extremely low, such that the Michaelis-Menten constant is much higher than the substrate concentration, the

nonlinear decomposition kinetics will converge to linear kinetics with respect to the substrate (Lasaga 1998, Wilson and Gerber 2021).

While simulations by structurally distinctive models with different parameterizations present a range of possibilities under specific theories and assumptions, calibrating model simulations against observational data helps identify the most probable mechanistic explanation that fits reality. Data assimilation is a suite of techniques that compare the model simulation results with different parameterizations against observed counterparts and adjust the model parameter values to the set with which the process-based model simulations best fit observations (Luo et al. 2011). Conventional data assimilation techniques such as Bayesian inference-based Markov Chain Monte Carlo (MCMC) method have been used at the site level to tune process-based models to better simulate soil carbon cycle (Xu et al. 2006, Li et al. 2016). Recently, the newly developed PROcess-guided deep learning and DAta-driven modeling (PRODA) approach (Tao and Luo 2022) integrates the site-level MCMC-based data assimilation results with deep learning to optimize the parameterization for global SOC simulations and reveals key mechanisms underlying SOC storage (Tao et al. 2020, Tao et al. 2023b). Here we hypothesize that with the same external forcing and observational constraint, simulations on global SOC by two models of different structures (i.e., CLM5 and COMPAS, see Methods below for detailed descriptions) can converge after being optimized by the PRODA approach. The convergence in simulating SOC will be achieved from the well-calibrated key processes in the soil carbon cycle despite structural differences among process-based models. Meanwhile, results of PRODA-optimized model simulation can also identify the most probable model structure that best fit observed SOC data across the globe.

2. Materials and Methods

2.1. Global vertical soil organic carbon profiles

We obtained soil organic carbon data in globally distributed soil profiles from the World Soil Information Service (WoSIS) and other data sources. WoSIS compiled soil data, after quality assessment, from soil profiles distributed across 173 countries (Batjes et al. 2020). The 2019 snapshot of the WoSIS dataset consists of 111,380 soil profiles with SOC content information (unit: g C kg^{-1} soil). We estimated the SOC stock (g C m^{-3}) by $SOC\ Stock = SOC\ Content \times BD$ (Yigini et al. 2018), where BD is the bulk density of soil (g m^{-3}). Note that SOC stock were multiplied by $1 - \frac{G}{100}$ to account for the volumetric coarse fragment fraction (G, unit: %) at each grid of the global map (data source: SoilGrids, https://soilgrids.org). When the measured bulk density was absent in the dataset, we used a pedo-transfer function to estimate it (Grigal et al. 1989, Yigini et al. 2018): $BD = \alpha + \beta \times \exp(-\gamma \times OM)$, where OM is organic matter, calculated as SOC×1.724, with SOC content in per cent (%); α, β, and γ are fitting parameters. After fitting data of WoSIS (i.e., 78,913 layers from 16,248 profiles that simultaneously recorded bulk density and SOC content) to this equation, we obtained α = 0.32, β = 1.30, and γ = 0.0089. The pedo-transfer function explained 55% of the variation in the bulk density. In addition, we obtained data from a previous study (Mishra et al. 2020) and the Northern Circumpolar Soil Carbon Database (NCSCD) (Hugelius et al. 2013). This dataset contained 2,546 soil profiles with SOC stock (g C m^{-3}) information for permafrost regions in North America, northern Eurasia, and Qinghai-Tibet Plateau. In total, we obtained data from 113,926 soil profiles as the raw data. The geographical distributions of all soil profiles are shown in Supplementary Figure 1.

Not all the soil profiles are used in this study. We pre-processed the 113,926 SOC profiles to ensure the quality of the data before we conducted our analysis. We first excluded SOC profiles with no more than two observation layers or the maximum observation depths

of no deeper than 50 cm from this study as such data do not provide enough information on key processes underlying SOC storage. After that, we obtained 72,377 profiles.

To further examine the quality of data along the vertical profiles, we conducted data assimilation for each of the 72,377 SOC vertical profiles with both the Community Land Model version 5 (CLM5) and the CarbOn cycle and Microbial PArtitioning Soil model (COMPAS) using the Markov Chain Monte Carlo (MCMC) method. Model structures of CLM5 and COMPAS are described in sections 4.2 and 4.3, respectively. The method of data assimilation is briefly described in section 4.4 below and in detail by Tao et al. (2020).

We used two statistics (i.e., G-R statistic and Nash-Sutcliffe modelling efficiency coefficient) to ensure the quality of calibration against SOC data along the vertical profiles. We calculated the Gelman-Rubin (G-R) statistic (Gelman et al. 2014) for each of the SOC profiles to test the convergence of the site-level data assimilation results after running three independent series of MCMC simulations (see Section 2.6 for details of MCMC). A G-R value approaching 1.0 suggests well converged data assimilation results. A large G-R value, in contrast, indicates inconsistent data assimilation results from independent MCMC simulations, and such results may not be trusted. Therefore, we set a threshold of G-R = 1.05 and excluded SOC profiles with G-R > 1.05 from our analysis in this study. The remaining 66,935 profiles for CLM5 and 59,476 for COMPAS went through the next analysis below. We found it was more difficult for independent MCMC simulations to converge when using COMPAS model in data assimilation, probably because of its nonlinearity. Thus, the final adopted profiles for COMPAS are fewer than those for CLM5.

We used the Nash-Sutcliffe modelling efficiency coefficient (Janssen and Heuberger 1995) (NSE) to evaluate the effectiveness of retrieving information from observations by process-based models. NSE is expressed as:

$$NSE = 1 - \frac{\sum(obs_i - mod_i)^2}{\sum(obs_i - \overline{obs_i})^2} \qquad (1).$$

A value of NSE close to 1 indicates that SOC distributions with depth can be well captured by process-based models so that information contained in the observations can be retrieved to evaluate processes underlying SOC storage. A small value of NSE indicates that the model cannot capture the variability in the data, suggesting that such SOC vertical profiles may not offer enough information on the processes underlying SOC storage investigated in this study. We set a threshold NSE = 0.0 to exclude SOC profiles from the analysis. We randomly selected a subset of these excluded SOC profiles to visually cross-check their shapes. We found that the thresholds are effective for controlling the quality of data.

After all the data pre-processing procedures, we eventually obtained data assimilation results from 62,931 soil profiles for CLM5 and 57,267 soil profiles for COMPAS with which we estimated global SOC storage and its components. Our data pre-processing criteria did not cause significant discrimination against profiles belonging to specific soil orders or ecosystems or different vertical shapes (Tao et al. 2023b). Thus the main conclusions drawn from this study are unlikely influenced by our data pre-processing criteria.

2.2. Model structure of CLM5

CLM5 is the latest version of the land model of the Community Earth System Model version 2 (CESM2) (Lawrence et al. 2018, Lawrence et al. 2019). SOC dynamics in CLM5 can be expressed in a uniform matrix equation (Huang et al. 2018, Lu et al. 2020, Luo et al. 2022):

$$\frac{d\boldsymbol{X}(t)}{dt} = \boldsymbol{B}I(t) + \boldsymbol{A}\xi(t)\boldsymbol{K}\boldsymbol{X}(t) + \boldsymbol{V}(t)\boldsymbol{X}(t) \qquad (2)$$

This matrix equation has six components (Supplementary Table 1), including plant carbon inputs ($I(t)$), carbon input allocation to different pools and depths ($\boldsymbol{B}$), substrate decomposability (or baseline decomposition rates) ($\boldsymbol{K}$), carbon transfer efficiency ($\boldsymbol{A}$), environmental modifier ($\boldsymbol{\xi}(t)$), and vertical transport ($\boldsymbol{V}(t)$).

CLM5 describes seven carbon pools in the soil, including four litter pools (i.e., coarse woody debris (indicated by subscript CWD), metabolic litter (ML), cellulose litter (CL), and lignin litter (LL)) and three soil organic carbon pools (i.e., active (aSOC), slow (sSOC), and passive (pSOC) soil organic carbon pools). Each of the carbon pools is simulated at 20 layers to a maximum depth of 8.4 m. The state of different carbon pools (i.e., carbon stocks) can be expressed as:

$$\boldsymbol{X}(t) = \begin{bmatrix} \boldsymbol{x}_{CWD}(t) \\ \boldsymbol{x}_{ML}(t) \\ \boldsymbol{x}_{CL}(t) \\ \boldsymbol{x}_{LL}(t) \\ \boldsymbol{x}_{aSOC}(t) \\ \boldsymbol{x}_{sSOC}(t) \\ \boldsymbol{x}_{pSOC}(t) \end{bmatrix} \quad (3)$$

where each of the 7 block elements (i.e., $\boldsymbol{x}_i(t)$) of $\boldsymbol{X}$(t) has 20 elements to represent the 20 soil layers. In total, CLM5 simulates carbon transfer among 140 pools. Consequently, there are 140 dimensions for vector $\boldsymbol{B}$ of carbon input allocation, matrix $\boldsymbol{K}$ of substrate decomposability, matrix $\boldsymbol{A}$ of carbon transfer from one carbon pool to another, matrix $\boldsymbol{\xi}(t)$ of environmental modifiers, and matrix $\boldsymbol{V}(t)$ of vertical transport. Plant carbon input ($I(t)$) is a scalar. In this study, parameters (Supplementary Table 1) that generate the above elements in the matrix equation will be optimised by the PRODA approach.

Specifically, $I(t)$ is allocated to different litter pools in different layers along the soil profile via the allocation vector $\boldsymbol{B}$. Organic carbon in pool vector $\boldsymbol{X}(t)$ is decomposed following first-order kinetics as described by matrix $\boldsymbol{K}$:

$$\boldsymbol{K} = \begin{pmatrix} \boldsymbol{k}_{CWD} & & & & & & \\ & \boldsymbol{k}_{ML} & & & & & \\ & & \boldsymbol{k}_{CL} & & & & \\ & & & \boldsymbol{k}_{LL} & & & \\ & & & & \boldsymbol{k}_{aSOC} & & \\ & & & & & \boldsymbol{k}_{sSOC} & \\ & & & & & & \boldsymbol{k}_{pSOC} \end{pmatrix} \quad (4)$$

where $\boldsymbol{k}_i$ is independent from the state of its corresponding substrate $\boldsymbol{x}_i(t)$. Moreover, we used the environmental modifier (i.e., $\boldsymbol{\xi}(t)$) to account for the effects of environmental conditions on the decomposition processes. $\boldsymbol{\xi}(t)$ is calculated from functions of soil temperature ($\boldsymbol{\xi}_T$), soil water potential ($\boldsymbol{\xi}_W$), nitrogen and oxygen availability ($\boldsymbol{\xi}_{N-O}$), and soil depth ($\boldsymbol{\xi}_D$).

Organic carbon from any carbon pool is further partitioned by either microbial or non-microbial processes between a receiver carbon pool and CO_2 released to the atmosphere. All these processes can be summarised in the $\boldsymbol{A}$ matrix:

$$\boldsymbol{A} = \begin{bmatrix} \boldsymbol{-1} & \boldsymbol{0} & \boldsymbol{0} & \boldsymbol{0} & \boldsymbol{0} & \boldsymbol{0} & \boldsymbol{0} \\ \boldsymbol{0} & \boldsymbol{-1} & \boldsymbol{0} & \boldsymbol{0} & \boldsymbol{0} & \boldsymbol{0} & \boldsymbol{0} \\ \boldsymbol{a}_{CL,CWD} & \boldsymbol{0} & \boldsymbol{-1} & \boldsymbol{0} & \boldsymbol{0} & \boldsymbol{0} & \boldsymbol{0} \\ \boldsymbol{a}_{LL,CWD} & \boldsymbol{0} & \boldsymbol{0} & \boldsymbol{-1} & \boldsymbol{0} & \boldsymbol{0} & \boldsymbol{0} \\ \boldsymbol{0} & \boldsymbol{a}_{aSOC,ML} & \boldsymbol{a}_{aSOC,CL} & \boldsymbol{0} & \boldsymbol{-1} & \boldsymbol{a}_{aSOC,sSOC} & \boldsymbol{a}_{aSOC,pSOC} \\ \boldsymbol{0} & \boldsymbol{0} & \boldsymbol{0} & \boldsymbol{a}_{sSOC,LL} & \boldsymbol{a}_{sSOC,aSOC} & \boldsymbol{-1} & \boldsymbol{0} \\ \boldsymbol{0} & \boldsymbol{0} & \boldsymbol{0} & \boldsymbol{0} & \boldsymbol{a}_{pSOC,aSOC} & \boldsymbol{a}_{pSOC,sSOC} & \boldsymbol{-1} \end{bmatrix} \quad (5)$$

where all the block elements in the $\boldsymbol{A}$ matrix ($\boldsymbol{a}_{i,j}$) are diagonal matrices with the dimension of 20. a_{ij} represents the carbon transfer fraction from the donor (j) pool to the recipient (i) pool (see carbon transfer flows in **Figure 1**). Note that CLM5 does not differentiate carbon transfers mediated by microbial processes from those mediated by non-microbial processes (e.g., organo-mineral interactions). Thus, $\boldsymbol{a}_{i,j}$ in Equation 8 is a integrative value reflecting carbon transfers contributed by both microbial and non-microbial processes.

The transport matrix $\boldsymbol{V}$ of CLM5 is a tridiagonal matrix and describes vertical carbon movement between adjacent soil layers within the same carbon pool via bioturbation and cryoturbation. At steady state, the analytical solution of SOC stock by CLM5 was calculated as $\boldsymbol{X_{steady\ state}} = \left[\boldsymbol{A}\overline{\xi(t)}\boldsymbol{K} + \overline{\boldsymbol{V}(t)}\right]^{-1}\left[-\boldsymbol{B}\overline{\boldsymbol{I}(t)}\right]$, where the overbars indicate the mean values of related matrices ($\xi(t)$ and $\boldsymbol{V}(t)$) and scalar ($\boldsymbol{I}(t)$) over the period of forcing data. The

matrix representation for process-based soil carbon cycle models has been described in detail by Huang et al. (2018), Lu et al. (2020), and Luo et al. (2022).

2.3. Structure of COMPAS model

The CarbOn cycle and Microbial PArtitioning Soil (COMPAS) model follows the same structure proposed by (Allison et al. 2010) for SOC dynamics, which is further embedded within the structure for 20-layered vertical soil profiles. The description of vertical layers was adopted from CLM5. Organic carbon dynamics represented by COMPAS can be expressed by the same matrix framework as shown in Equation 2 (Supplementary Table 2). Yet COMPAS structurally differs from CLM5 in classifying soil carbon pools, expressing substrate decomposition, and explicitly describing microbial partitioning processes in carbon transfer.

Equation 2 describes COMPAS with 160 dimensions to represent 8 pools in each of the 20 soil layers. Vector $\boldsymbol{X}(t)$ has 8 block elements to represent four litter carbon pools (indicated by subscripts CWD, ML, CL, and LL) and four soil organic carbon pools (i.e., dissolved organic carbon (DOC), mineral-associated soil organic carbon (mSOC), microbial biomass (MIC), and extracellular enzymes (ENZ)):

$$\boldsymbol{X}(t) = \begin{bmatrix} \boldsymbol{x}_{CWD}(t) \\ \boldsymbol{x}_{ML}(t) \\ \boldsymbol{x}_{CL}(t) \\ \boldsymbol{x}_{LL}(t) \\ \boldsymbol{x}_{DOC}(t) \\ \boldsymbol{x}_{MIC}(t) \\ \boldsymbol{x}_{ENZ}(t) \\ \boldsymbol{x}_{mSOC}(t) \end{bmatrix} \quad (6)$$

Each of the 8 block elements (i.e., $\boldsymbol{x}_i(t)$) of $\boldsymbol{X}$(t) has 20 elements to represent the 20 soil layers. Similarly, there are 160 dimensions for vector $\boldsymbol{B}$, matrix $\boldsymbol{K}$, matrix $\boldsymbol{A}$, matrix $\boldsymbol{\xi}(t)$, and matrix $\boldsymbol{V}(t)$. Plant carbon input ($I(t)$) is still a scalar as in CLM5. Parameters

(Supplementary Table 2) that generate the above elements in the matrix equation will be optimised by the PRODA approach.

Different from CLM5, organic carbon pools in vector $\boldsymbol{X}(t)$ of COMPAS can be transferred to recipient pools either through microbial- or enzyme-mediated kinetics, or without going through microbial metabolism. These transfers are described by the baseline decomposition matrix $\boldsymbol{K}$:

$$\boldsymbol{K} = diag\begin{pmatrix} \boldsymbol{k}_{CWD} \\ \boldsymbol{k}_{ML} \\ \boldsymbol{k}_{CL} \\ \boldsymbol{k}_{LL} \\ \boldsymbol{k}_{DOC}(\boldsymbol{x}_{DOC}, \boldsymbol{x}_{MIC}) \\ \boldsymbol{k}_{MIC} \\ \boldsymbol{k}_{ENZ} \\ \boldsymbol{k}_{mSOC}(\boldsymbol{x}_{mSOC}, \boldsymbol{x}_{ENZ}) \end{pmatrix} \quad (7)$$

While all the litter organic carbon pools and two mineral organic carbon pools (i.e., MIC and ENZ) are decomposed following first-order kinetics where their baseline decomposition rates are constants, the baseline decomposition rates of DOC and mSOC are functions of carbon pool states. Specifically, the baseline decomposition rate of DOC (a.k.a. the baseline rate of microbial assimilation of DOC) is: $\boldsymbol{k}_{DOC}(\boldsymbol{x}_{DOC}, \boldsymbol{x}_{MIC}) = \frac{v_{max,assim}\boldsymbol{x}_{MIC}}{K_{m,assim}\boldsymbol{\xi}+\boldsymbol{x}_{DOC}}$; the baseline decomposition rate of mSOC is: $\boldsymbol{k}_{mSOC}(\boldsymbol{x}_{mSOC}, \boldsymbol{x}_{ENZ}) = \frac{v_{max,decom}\boldsymbol{x}_{ENZ}}{K_{m,decom}\boldsymbol{\xi}+\boldsymbol{x}_{mSOC}}$. Parameters $v_{max,assim}$ and $v_{max,decom}$ represent the maximum DOC assimilation and mSOC decomposition rates, respectively. $K_{m,assim}$ and $K_{m,decom}$ are the Michaelis constants for DOC assimilation and mSOC decomposition, respectively.

The COMPAS model also explicitly differentiates carbon transfers in microbial processes from those in non-microbial processes. The decomposed organic carbon is either partitioned by microorganisms to microbial biomass growth versus respiration (i.e., according to the microbial CUE), or alternatively, transferred to other carbon pools with a fraction that

is not mediated by microbial processes (i.e., non-microbial carbon transfer). All these processes are summarised in the $\boldsymbol{A}$ matrix:

$$\boldsymbol{A}=\begin{bmatrix} \mathbf{-1} & \mathbf{0} & \mathbf{0} & \mathbf{0} & \mathbf{0} & \mathbf{0} & \mathbf{0} & \mathbf{0} \\ \mathbf{0} & \mathbf{-1} & \mathbf{0} & \mathbf{0} & \mathbf{0} & \mathbf{0} & \mathbf{0} & \mathbf{0} \\ \boldsymbol{a}_{CL,CWD} & \mathbf{0} & \mathbf{-1} & \mathbf{0} & \mathbf{0} & \mathbf{0} & \mathbf{0} & \mathbf{0} \\ \boldsymbol{a}_{LL,CWD} & \mathbf{0} & \mathbf{0} & \mathbf{-1} & \mathbf{0} & \mathbf{0} & \mathbf{0} & \mathbf{0} \\ \mathbf{0} & \boldsymbol{a}_{DOC,ML} & \boldsymbol{a}_{DOC,CL} & \mathbf{0} & \mathbf{-1} & \boldsymbol{a}_{DOC,MIC} & \mathbf{1} & \boldsymbol{a}_{DOC,mSOC} \\ \mathbf{0} & \boldsymbol{a}_{MIC,ML} & \boldsymbol{a}_{MIC,CL} & \boldsymbol{a}_{MIC,LL} & \boldsymbol{a}_{MIC,DOC} & \mathbf{-1} & \mathbf{0} & \mathbf{0} \\ \mathbf{0} & \mathbf{0} & \mathbf{0} & \mathbf{0} & \mathbf{0} & \boldsymbol{a}_{ENZ,MIC} & \mathbf{-1} & \mathbf{0} \\ \mathbf{0} & \mathbf{0} & \mathbf{0} & \boldsymbol{a}_{mSOC,LL} & \mathbf{0} & \boldsymbol{a}_{mSOC,MIC} & \mathbf{0} & \mathbf{-1} \end{bmatrix} \quad (8)$$

Because DOC is always assimilated by the microbes with release of CO_2 (**Figure 1**), the microbial CUE for DOC (η_{DOC}) equals $\boldsymbol{a}_{MIC,DOC}$. In contrast, organic carbon in the metabolic, cellulose, and lignin litter pools is decomposed by microbes following first-order kinetics to generate CO_2 and grow biomass while a fraction of litter organic carbon is broken down without going through microbial metabolism and, thus, directly transferred to DOC or mSOC. In this case, the microbial CUE for the three litter carbon pools can still be expressed as: $\eta_{ML}=\frac{\boldsymbol{a}_{MIC,ML}}{1-\boldsymbol{a}_{DOC,ML}}$, $\eta_{CL}=\frac{\boldsymbol{a}_{MIC,CL}}{1-\boldsymbol{a}_{DOC,CL}}$, and $\eta_{LL}=\frac{\boldsymbol{a}_{MIC,LL}}{1-\boldsymbol{a}_{mSOC,LL}}$, respectively.

COMPAS applies the same approach to simulate carbon input allocation (B), environmental modifier (i.e., $\boldsymbol{\xi}(t)$) and transport matrix $\boldsymbol{V}$ as those used in CLM5. It should be noted that while COMPAS and CLM5 use the same scheme to simulate B, $\boldsymbol{\xi}(t)$, and $\boldsymbol{V}$, parameter values (Supplementary Tables 1-2) that were used to calculate the above elements in the matrix equation were estimated independently by the PRODA approach.

In calculating the steady state of different carbon pools by COMPAS, Equation 2 can be separated into two equations: one for litter carbon cycle and the other for mineral SOC cycle, because there is no carbon transfer from mineral soil carbon pools to litter carbon pools (i.e., $\boldsymbol{a}_{litter\ pool,soil\ pool}=\mathbf{0}$ in the $\boldsymbol{A}$ matrix). Since $\boldsymbol{A}$, $\boldsymbol{K}$, $\boldsymbol{\xi}(t)$, and $\boldsymbol{V}$ are all independent from litter carbon pool states (i.e., $\boldsymbol{X}$), the analytical solution of litter carbon stock at the steady state (SS) can be calculated as $\boldsymbol{X}_{litter,SS}=\left[\boldsymbol{A}_{litter}\overline{\boldsymbol{\xi}(t)_{litter}}\boldsymbol{K}_{litter}+\right.$

$\overline{\boldsymbol{V}(t)_{litter}}\Big]^{-1}\Big[-\boldsymbol{B}_{litter}\overline{\boldsymbol{I}(t)_{litter}}\Big]$. For the soil organic carbon pools, the related $\boldsymbol{K}$ matrix is carbon pool state dependent (see Equation 7). We assumed there is no vertical transport for soil organic carbon pools such that litter is added to different soil layers and transported vertically, and then it is transferred to soil pools that are immobile in that layer. According to a method reported by Georgiou et al. (2017), the steady-state solutions for soil organic carbon pools are:

$$\boldsymbol{X}_{soil,SS}=\begin{bmatrix}\boldsymbol{x}_{DOC,SS}\\ \boldsymbol{x}_{MIC,SS}\\ \boldsymbol{x}_{ENZ,SS}\\ \boldsymbol{x}_{mSOC,SS}\end{bmatrix}=\begin{bmatrix}\dfrac{\boldsymbol{k}_{MIC}\boldsymbol{\xi}K_{m,assim}\boldsymbol{\xi}\boldsymbol{x}_{MIC,SS}-\boldsymbol{u}_{MIC}K_{m,assim}\boldsymbol{\xi}}{(\eta_{DOC}v_{max,assim}-\boldsymbol{k}_{MIC})\boldsymbol{\xi}\boldsymbol{x}_{MIC,SS}+\boldsymbol{u}_{MIC}}\\ \dfrac{\boldsymbol{u}_{MIC}+\eta_{DO\square\square}(\boldsymbol{u}_{mSOC}+\boldsymbol{u}_{DOC})}{(1-\eta_{DOC})\boldsymbol{k}_{MIC}\boldsymbol{\xi}}\\ \dfrac{\boldsymbol{a}_{ENZ,MIC}\boldsymbol{k}_{MIC}\boldsymbol{x}_{MIC,SS}}{\boldsymbol{k}_{ENZ}}\\ \dfrac{\big(\boldsymbol{u}_{mSOC}+\boldsymbol{a}_{mSOC,MIC}\boldsymbol{k}_{MIC}\boldsymbol{\xi}\boldsymbol{x}_{MIC,SS}\big)K_{m,decom}\boldsymbol{\xi}}{(v_{max,decom}\boldsymbol{\xi}\boldsymbol{x}_{ENZ,SS}-\boldsymbol{a}_{mSOC,MIC}\boldsymbol{k}_{MIC}\boldsymbol{\xi}\boldsymbol{x}_{MIC,SS}-\boldsymbol{u}_{mSOC})}\end{bmatrix} \quad (9)$$

where $\boldsymbol{u}_{S_i}$ is the carbon input from litter pools (L_j) to a mineral soil carbon pool (S_i, see Extended Data Fig. 3 for corresponding carbon flows for each mineral soil carbon pool) and is expressed as $\sum_{L_j}\left(\boldsymbol{a}_{S_i,L_j}\boldsymbol{k}_{L_j}\boldsymbol{\xi}\boldsymbol{x}_{L_j}\right)$. Note that all the elements with bold font indicate vectors of the corresponding variables or parameters for the 20 soil layers. All the multiplications shown in Equation 12 are element-wise operations.

2.4. Inputs and environmental conditions

For both CLM5 and COMPAS, the carbon input for the litter carbon pools (i.e., net primary productivity, NPP) and environmental forcings (e.g., soil temperature and moisture) are from 20 years of monthly model outputs (Supplementary Table 3) by CLM5 at the steady state using a preindustrial forcing (i.e., I1850Clm50Bgc, from year 1901 to 1920) at 0.5-degree resolution. We used the 20-year annual mean values of different components in Equation 2 to calculate total soil organic carbon stock at steady state.

342

343 **2.5. Default (*ad hoc*) parameterizations**

344 We compared the model simulation results of CLM5 and COMPAS when applying default
345 parameterization and the parameterization optimised by the PRODA approach. For CLM5,
346 we applied the parameter values used in its current version (Lawrence et al. 2019). In the
347 default scheme, most of the selected 21 parameters of CLM5 are constants across the globe,
348 except two carbon transfers that are sand content dependent, and the parameter controlling
349 plant carbon input allocation that depends on plant functional types (**Supplementary Table**
350 **1**). For COMPAS, it is a newly constructed model and thus does not have well-tuned
351 parametrization for global simulation. We applied the global mean values of the selected 23
352 parameters after site-level data assimilation as the default parameterization for COMPAS to
353 drive the global simulation.

354

355 **2.6. PROcess-guided deep learning and DAta-driven modelling (PRODA)**

356 The PRODA approach integrates big data with Bayesian data assimilation and deep learning
357 to optimize soil carbon cycle simulation with process-based models (Tao and Luo 2022). We
358 used the PRODA approach to optimize both CLM5 and COMPAS at the global scale. Data
359 assimilation was first applied at each SOC profile to estimate parameter values. 21
360 parameters for CLM5 and 23 parameters for COMPAS were optimised for each SOC profile
361 so that the process-based model simulations can best fit local observations. Because we
362 conducted data assimilation independently at each observational site, optimised values of the
363 same parameter vary across space. We further used a neural network to generalise those
364 estimated parameter values after the site-level data assimilation to the global scale by a neural
365 network. The global parameter maps predicted by the neural network were then used in the

process-based models to simulate global SOC storage and retrieve the spatial patterns of related model components over the globe.

We conducted Bayesian data assimilation by using the MCMC method for each of the SOC profiles to estimate the parameter values of the process-based models that best fit model simulations with SOC observations. Because the soil profile data collected from field measurement of soil organic carbon includes all components of the organic matter (e.g., microbial biomass carbon), we used the sum of modeled mineral soil carbon pools classified in CLM5 and COMPAS to be compared with soil profile data.

Specifically, at site-level data assimilation, for each SOC profile, we applied an adaptive Metropolis algorithm (Haario et al. 2001) to generate the posterior distributions of a total of 21 parameters of CLM5 (Supplementary Table 1) and 23 parameters of COMPAS (Supplementary Table 2) related to six model components with two phases of simulations (i.e., a test run and a formal run). We first conducted a test run assuming uniform distributions for each of the preselected parameters as the proposal distributions (i.e., prior knowledge). The prior ranges of the uniform distributions for each parameter are shown in Supplementary Tables 1-2. The proposal distributions continuously generated a set of parameter values for the process-based models to simulate SOC storage. We then judged whether the proposed parameter values should be accepted or not by comparing their model simulation results with SOC observations. In the formal run, we used the accepted sets of parameter values obtained in the test run as the proposal distributions and assumed that all the target parameters are multivariate Gaussian distributed. We proposed new sets of parameter values and judged them to be accepted or not following the same rule in the test run. Unlike the test run, the proposal distributions in the formal run were continuously adjusted according to the newly accepted sets of parameters.

We set 20,000 iterations for the test run and 50,000 iterations for the formal run. Eventually, we controlled the acceptance ratio (i.e., the ratio of accepted sets of parameters out of the total number of iterations) of the formal run between 10% and 50%. We set the burn-in coefficient as 50%, where the first half of the accepted parameter values in the formal run was discarded, and the second half was used to generate the posterior distributions of parameters. We calculated the mean values of the posterior distributions of parameters as the final point estimates. We ran three independent series of MCMC for each SOC profile and calculated the G-R statistic to test the convergence of data assimilation results. The mean G-R values of the target parameters were further calculated as the holistic performance of MCMC for each SOC profile. The mathematical foundations of Bayesian data assimilation and technical details of the MCMC method were documented by Tao et al. (2020).

It should be noted that the data assimilation was conducted under the assumption that SOC profiles are at steady state (i.e., $\frac{\mathrm{d}\mathbf{X}(\mathrm{t})}{\mathrm{dt}} = 0$). This assumption makes data assimilation computationally more feasible than that under non-steady state (see the non-steady-state data assimilation in Zhou et al. (2023) and Zhou et al. (2015)). While soil carbon stocks in some ecosystems (e.g., agricultural soils) may not be at the steady state because of the concurrent climate change and human activities, previous research demonstrated that such disequilibrium component of the transient carbon cycle dynamics, especially in SOC pools, is minor in comparison with the amount of SOC storage that was developed over thousands of years (Lu et al. 2018).

We trained a fully connected multilayer neural network to predict the site-level parameter values estimated from data assimilation with a suite of 60 environmental variables (Supplementary Table 4). To achieve better training effectiveness, we first normalized all the environmental variables and parameters to the interval of [0, 1] according to their maximum and minimum values. We then conducted a set of pre-experiments to determine the best

415 configuration setting of the neural network. The neural network used in the final training
416 consisted of four hidden layers. The node numbers for each hidden layer were 256, 512, 512,
417 and 256, respectively. We used a rectified linear unit (ReLU) as the activation function and a
418 gradient descent optimization algorithm (adadelta) as the optimizer. The loss function was
419 designed as the multiplication of L1 (i.e., ratio loss: $RL = \frac{\sum_{i=1}^{N}\left|\frac{para_{i,true}-para_{i,pred}}{para_{i,true}}\right|}{N}$) and L2
420 (i.e., mean squared error: $MSE = \frac{\sum_{i=1}^{N}(para_{i,true}-para_{i,pred})^2}{N}$) errors, where $para_{i,true}$ is the
421 *i*th parameter value optimized in the site-level data assimilation, $para_{i,pred}$ is the *i*th
422 parameter predicted by the neural network, and *N* is the total number of parameters of the
423 process-based models to be predicted by the neural network (*N* = training size × 23 for
424 COMPAS and training size × 21 for CLM5).. We decided to use this composite $L1 \times L2$ loss
425 function because training with either L1 or L2 loss alone did not yield sufficient prediction
426 accuracy. The batch size for each iteration of optimization was 32. We set a maximum of
427 6,000 epochs to train the neural network and selected the model with the lowest validation
428 loss as the final training result. To avoid overfitting in training the neural network, we set a
429 drop-out ratio of 20% for each of the hidden layers.
430
431 **2.7. Global maps of SOC, residence time, and related model components**
432 Global maps of parameters that were predicted by the best-guess neural network using the
433 gridded environmental variables were applied to the two process-based models to generate
434 global maps of SOC storage and its related components (i.e., 57,267 sets of site-level data
435 assimilation results for COMPAS and 62,931 for CLM5).
436 We retrieved the system-level carbon transfer efficiency (CTE), plant carbon inputs,
437 allocation of input carbon to different soil layers, substrate decomposability, environmental
438 modifications, and vertical transport from the optimized parameters of COMPAS and CLM5

(Supplementary Tables 1-2) via the PRODA approach. All the six model components referred to in this study are ensembles of processes that were represented by different parameters in the process-based model. Note that all the system-level components discussed in this study are for the soil system that integrates both litter organic carbon and mineral soil organic carbon.

Specifically, we calculated the system level carbon transfer efficiency as the sum of carbon transfer coefficients along each carbon transformation pathway (i.e., a_{ij} in Equation 3) weighted by the carbon fluxes over all the pathways in the soil system:

$$CTE_{system} = \sum_{ij} a_{ij} \frac{\sum_z x_{j,z} k_j \xi_z \Delta z}{\sum_j \sum_z x_{j,z} k_j \xi_z \Delta z} \qquad (10)$$

where a_{ij} represents the carbon transfer fraction from the donor (j) pool to the recipient (i) pool; $x_{j,z}$ is the carbon pool size at depth z (g C m^{-3}); k_j is the depth-independent baseline decomposition rate (yr^{-1}) of the corresponding carbon pool; ξ_z represents the environmental modifier at depth z; and Δz is the thickness of zth soil layer. Note that CTE along the carbon transfer pathway to recipient pool i from donor pool j (i.e., a_{ij}) is weighted by the flux size from donor pool j (i.e., $\sum_z x_{j,z} k_j \xi_z \Delta z$), which measures the amount of decomposed carbon along the j to i transfer pathway, normalized by the total flux in the soil system (i.e., $\sum_j \sum_z x_{j,z} k_j \xi_z \Delta z$). A higher CTE value indicates a larger amount of carbon remaining in the recipient soil pool after organic carbon is decomposed or transformed by biological and/or chemical and physical reactions, which, by definition, also associates with less CO_2 released back to the atmosphere.

The baseline decomposition rate (unit: yr^{-1}) expresses the rate of organic carbon decomposition at optimal soil temperature and water conditions. We calculated the system-level baseline decomposition rate (K_{system}, unit: yr^{-1}) by weighting the baseline decomposition rate of SOC pools by their carbon pool sizes:

$$K_{bulk} = \sum_i k_i \frac{x_i}{\sum x_i} \qquad (11)$$

Similarly, we weighted the vertical transport rate (yr^{-1}) and environmental modifiers (unitless) at different soil depths (z) by their corresponding sizes of SOC stock (i.e., x_z, with unit of g C m^{-2}):

$$V_{system} = \sum_z \left(v_z \frac{x_z}{\sum x_z} \right) \qquad (12)$$

$$\xi_{system} = \sum\nolimits_z \left(\xi_{T,z} \xi_{W,z} \xi_{D,z} \frac{x_z}{\sum x_z} \right) \qquad (13)$$

Carbon input is distributed vertically according to the distribution of root biomass at different soil depths (Jackson et al. 1996). Therefore, to quantify how effectively the input allocation process distributes litterfall and root exudation to different soil depths, we calculated the fraction of carbon input allocated to soils layers below 5 cm as the system-level index for plant carbon input allocation:

$$B_{system} = \left[\frac{\sum_z exp\left[\frac{ln(1 - Y_z)}{D_z} \right]}{n} \right]^5 \qquad (14)$$

where Y_z is the cumulative fraction of input carbon at soil depth of D_z; n is the number of soil layers. A larger system-level input allocation index indicates that more carbon from litterfall and root exudation will be allocated to deeper soils. This index differs between models because the parameters describing the vertical distribution of carbon inputs are optimized independently in the two models, even if we used the simulated total litterfall (equivalent to the net primary productivity, NPP) in CLM5 as the plant carbon input for both models.

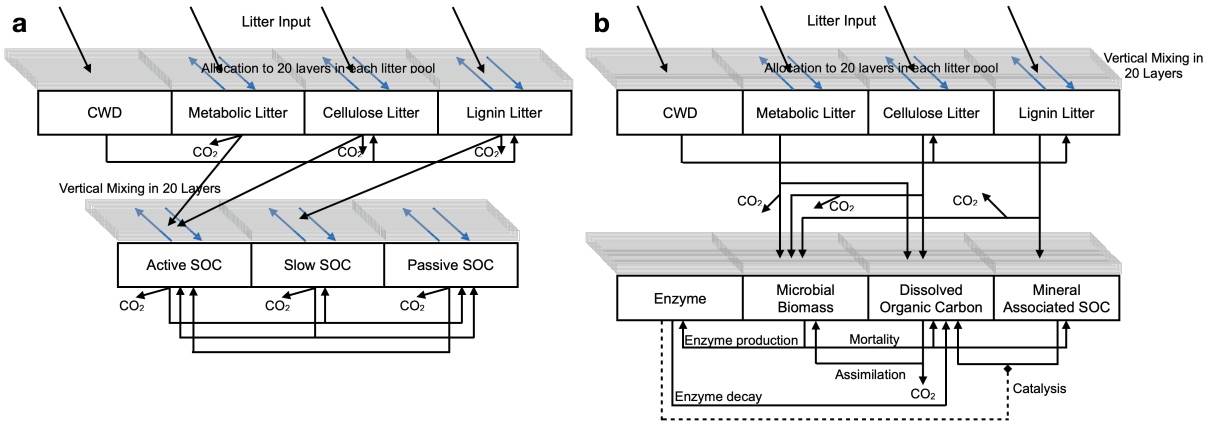

Figure 1. Distinctive model structures of CLM5 (a) and COMPAS (b).

3. Results

Process-based models with different structures and *ad hoc* parameterizations present diverging results in representing global SOC storage and spatial patterns. With its default parameterization, CLM5 simulates much more SOC in the boreal regions than tropics. In East Siberia and Alaska, SOC storage is more than 50 kg C m^{-2} for the first meter, whereas, in the Amazon and Congo basins and Indonesia, the average SOC storage is less than 10 kg C m^{-2} (**Figure 2a, c**). As COMPAS does not have well-tuned default parameter values at the global scale, we used the global mean values of the selected parameters after site-level data assimilation as the default parameterization. COMPAS with such *ad hoc* parameterization simulates distinctively different SOC patterns from CLM5 across latitudes. Tropical regions with the highest carbon input are simulated to store the largest amount of SOC. The average SOC storage declines from more than 20 kg C m^{-2} in Amazon, Congo, and Indonesia to less than 5 kg C m^{-2} in boreal regions (**Figure 2b-c**). The correlation between the simulated spatial patterns of SOC by CLM5 and COMPAS is -0.026 (logarithmically transformed SOC values, d.f. = 45,213, $P < 0.0001$). Despite the contrasting spatial patterns, both of the models reasonably estimate the total global SOC storage with their *ad hoc* parameterizations. CLM5 and COMPAS simulate 1281 Pg C and 1308 Pg C preserved as SOC for the first meter soils across the globe, respectively.

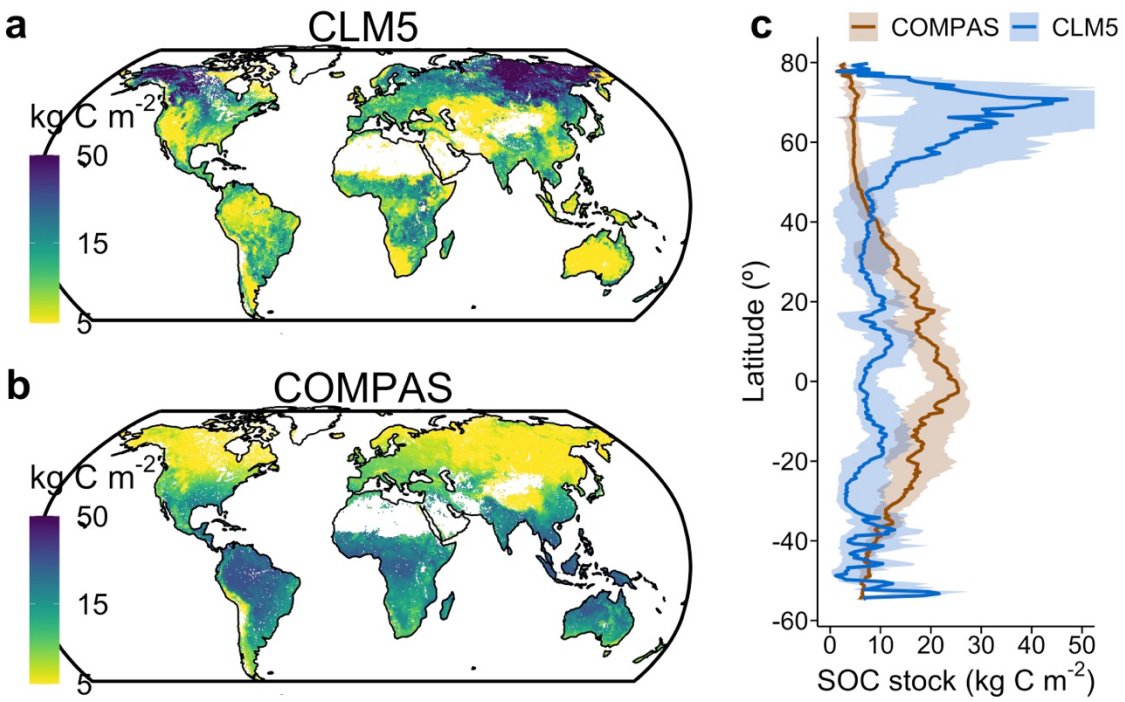

Figure 2. Diverging SOC simulation by structurally different models with *ad hoc* parameterization. (a) SOC estimated by CLM model, (b) SOC estimated by COMPAS, (c) latitudinal variation in estimated SOC by the two models.

After being constrained by the same SOC data using the PRODA approach, the two structurally different models simulate similar SOC storage and spatial patterns. At site-level, we found that posterior distributions of selected parameters after data assimilation could be very different from their default values (**Supplementary Figure 2**) and also differ from site to site. We further used PRODA to generalise the emerging spatial heterogeneity of optimised parameter values in site-level data assimilation to the global scale and found similar SOC simulations by CLM5 and COMPAS. Simulations by CLM5 continue to show higher SOC storage in the boreal regions than in the tropics. In addition to simulating higher SOC in East Siberian and Alaska, PRODA-optimised CLM5 also identifies western Siberian lowlands as areas holding high SOC storage (**Figure 3a, c**). Meanwhile, the simulated SOC storage in tropical regions, after being constrained by observations, is increased to an average value of

more than 10 kg C m^{-2} (**Figure 3b-c**). Simulation results by COMPAS after PRODA optimization now follow a pattern similar to that shown by CLM5. The correlation between simulations by COMPAS and CLM5 is 0.51 (logarithmically transformed SOC values, d.f. = 45,213, $P < 0.0001$). Notably, differences still exist in simulating sub-continental patterns by these two models. While both of the models simulate the highest SOC storage in western Siberian lowlands, Alaska, and Canadian Shield, COMPAS simulates more SOC in tropics but less SOC in East Siberian than CLM5. The total SOC storage simulated by COMPAS is slightly higher than that by CLM5. Globally, the total SOC storage in 1m depth estimated by PRODA-optimised CLM5 and COMPAS is 1469 Pg C and 1507 Pg C, respectively.

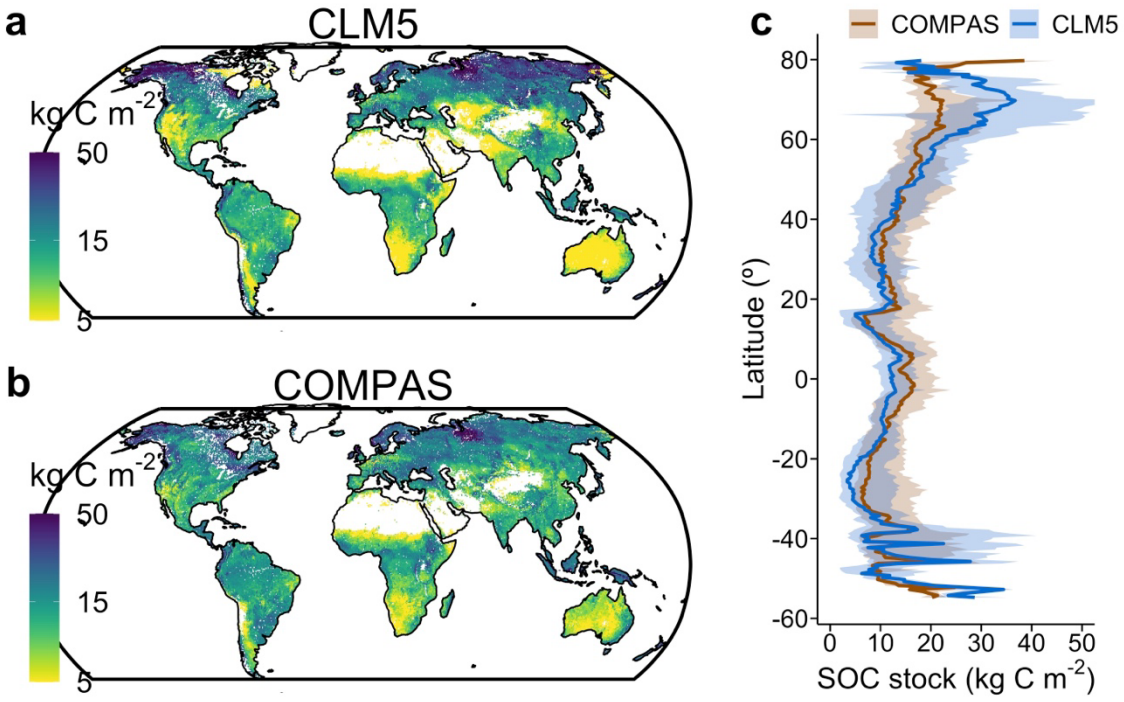

Figure 3. Converging SOC simulation by structurally different models after data model fusion by the PRODA approach. (a) SOC estimated by CLM model, (b) SOC estimated by COMPAS, (c) latitudinal variation in estimated SOC by the two models.

539 Simulations of key components related to SOC storage also converge after the two
540 structurally different models are constrained by the same set of SOC data (**Figure 4**). We
541 assessed the spatial patterns of six components simulated by the two models: carbon transfer
542 efficiency, baseline decomposition, environmental modifier, carbon input allocation, vertical
543 transport rate, and plant carbon input. The carbon transfer efficiency quantifies the ratio of
544 decomposed carbon being transferred from one carbon pool to another. CLM5 and COMPAS
545 represent the carbon transfer efficiency differently (**Figure 1**). COMPAS explicitly describes
546 microbial CUE that partitions the metabolized organic carbon into microbial biomass
547 accumulation versus respiration and the non-microbial carbon transfer related to the
548 transformation of carbon from one carbon pool to another via organo-mineral interactions
549 (**Figure 1b**). In contrast, CLM5 fuses microbial CUE and non-microbial carbon transfer in its
550 structure, such that the related parameters do not differentiate these two processes but
551 integrate their effects together in simulations (**Figure 1a**). Despite the difference in structure,
552 CLM5 and COMPAS simulate similar patterns of system-level carbon transfer efficiency
553 (**Figure 4c**, Pearson correlation coefficient = 0.52, d.f. = 45,228, $P < 0.001$) after being
554 constrained by the same observed SOC dataset. Both models show higher carbon transfer
555 efficiency in boreal regions than in the tropics (**Figure 4a-b**), which indicates that in boreal
556 regions, more carbon is maintained in the soil system after SOC is decomposed or
557 transformed by biological and/or chemical and physical reactions instead of being released
558 back to the atmosphere as CO_2.
559 The rate of SOC decomposition is determined by the substrate decomposability (as
560 indicated by the baseline decomposition) and modified by surrounding environmental factors
561 (i.e., soil temperature and water). A high baseline decomposition indicates the organic
562 substrate is chemically and physically more accessible to soil microorganisms (e.g., simpler
563 chemical compounds or weaker interactions with the soil mineral matrix), whereas a lower

564 environmental modifier value suggests the SOC decomposition is more restricted by either
565 low temperature or too much or little soil water. In this study, CLM5 and COMPAS,
566 respectively, assume first-order and Michaelis-Menten kinetics in representing SOC
567 decomposition. Notwithstanding their difference in kinetic assumptions, PRODA-optimised
568 CLM5 and COMPAS agree on the highest baseline decomposition rates and the lowest
569 environmental modifier values in boreal regions across the globe (**Figure 4d-i**). The
570 correlation coefficients between the simulations by the two models are 0.55 (d.f. = 45,228, P
571 < 0.001) for baseline decomposition and 0.80 (d.f. = 45,228, P < 0.001) for environmental
572 modifier.

573 However, not all components investigated in this study show convergence after data
574 assimilation. Vertical transport quantifies the rate of organic carbon moving from the surface
575 to deeper soil layers. The plant carbon allocation represents how the vertical distribution of
576 carbon inputs. While CLM5 and COMPAS adopt identical mathematical functions to
577 describe these two processes, no agreement was reached on simulated spatial patterns after
578 the related parameters of the two models were optimized by the PRODA approach (**Figure**
579 **4j-o**). Moreover, it should be noted that the retrieved model components using CLM5 and
580 COMPAS are usually outside the 1:1 line even when they are well correlated. While the two
581 models agree well on the magnitude of the simulated environmental modifier (**Figure 4i**), the
582 linear CLM5 simulates higher carbon transfer efficiency values (**Figure 4c**) but lower
583 baseline decomposition rates (**Figure 4f**) than the nonlinear COMPAS. This pattern may
584 occur because parameters related to carbon transfer efficiency and baseline decomposition
585 compensate each other in CLM5 and COMPAS for a similar SOC storage simulation. Even
586 though we used the same plant carbon input (i.e., the total amount of carbon from plant to
587 litter) from CESM2 outputs in simulating SOC storage by the two models (**Figure 4p-r**),
588 COMPAS and CLM5 simulated differently how carbon transfers from litter to mineral soils

(**Figure 1**), as quantified by the ratio between the amount of carbon transferred from litter to mineral soils and the total carbon input. COMPAS simulates larger amounts of litter carbon to be transferred to mineral soils than CLM5 (**Supplementary Figure 3**), which requires higher baseline decomposition rates of COMAS than CLM5 to reach similar SOC storage in SOC storage simulation, as shown in **Figure 4d-f**.

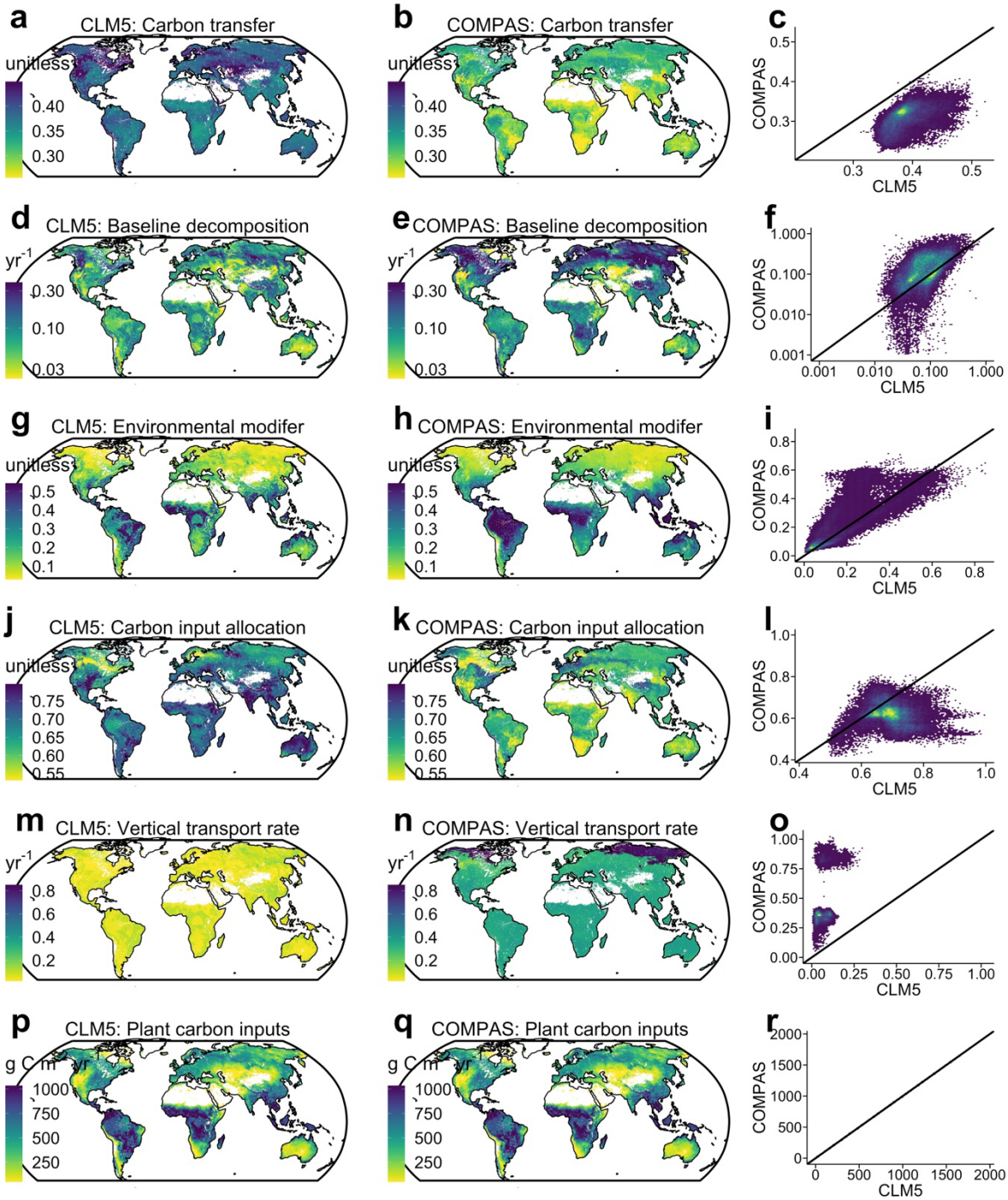

Figure 4. Spatial patterns of different model components retrieved by CLM (left column) and COMPAS (central column) models using the PRODA approach. The right column shows comparisons between the model components retrieved from the two models. The model components were: (a-c) carbon transfer efficiency, (d-f) baseline decomposition, (g-i) environmental modifier, (j-l) carbon input allocation, (m-o) vertical transport rate, and (p-r) plant carbon input.

The nonlinear decomposition kinetics in COMPAS can be approximated as first-order kinetics with respect to both donor and receiver carbon pools, after being constrained by observed SOC data. Compared with the linear first-order kinetics used in CLM5, COMPAS specifies the decomposition of SOC and assimilation of DOC as nonlinear Michaelis-Menten kinetics. Thus, the decomposition of substrates is determined by both the catalyst (i.e., microbes for DOC assimilation and enzyme for mSOC decomposition) and the substrate concentration (i.e., DOC for DOC assimilation and mSOC for mSOC decomposition). Mathematically, when the Michaelis constants (i.e., $K_{m,decom}$ and $K_{m,assim}$) are much larger (e.g., 100 times larger) than their corresponding substrate concentrations, the Michaelis-Menten kinetics becomes first-order kinetics with respect to DOC or SOC (but also with respect to MIC or ENZ, so that the rate equations are still nonlinear). After data assimilation at each SOC profile using COMPAS, we found that both $k_{m,decom}$ and $k_{m,assim}$ in the Michaelis-Menten equation are more than 100 times that of their substrate concentrations (i.e., SOC and DOC concentrations) for most of the soil profiles (**Figure 5**). Thus, the nonlinear kinetics for enzyme-based mSOC decomposition and microbe-based DOC assimilation can be approximated by first-order kinetics with respect to mSOC and DOC after COMPAS is constrained by globally distributed SOC vertical profiles. While losing the nonlinear character of the donor pool effect, these kinetics laws still retain the effect of microbial biomass or enzyme carbon, resulting in multiplicative kinetics.

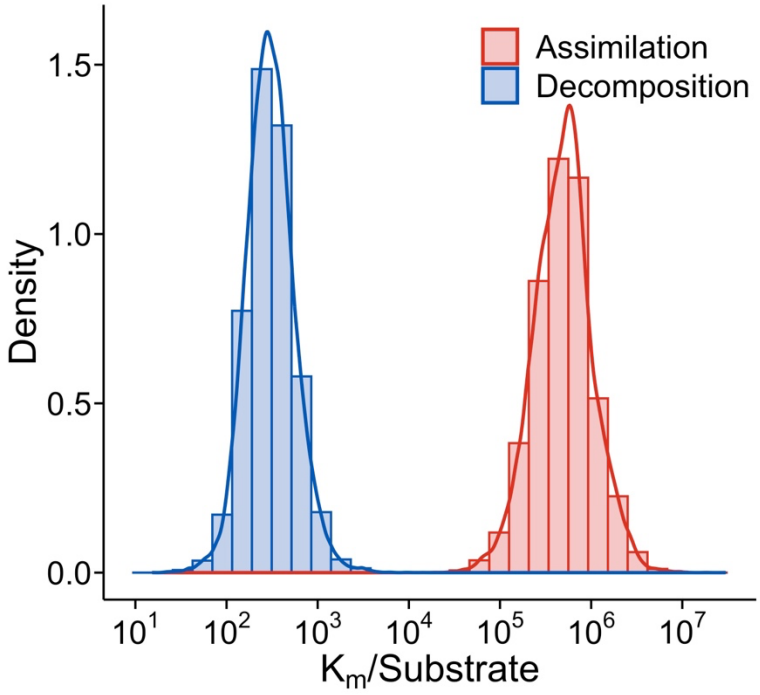

Figure 5. Relationship between Michaelis-Menten constants and their corresponding substrate content in COMPAS after being constrained by observational SOC profiles. For decomposition, 'Substrate' is mineral-associated organic carbon (mSOC) and $K_m = K_{m,decom}$; for assimilation, 'Substrate' is dissolved organic carbon (DOC) and $K_m = K_{m,assim}$.

4. Discussion

4.1. Data assimilation enables converged SOC simulations by structurally different models

The divergent simulations by process-based models with different structures and *ad hoc* parameterizations reflect large uncertainties in current understanding of soil carbon dynamics with different theories and assumptions. In this study, CLM5 and COMPAS structurally differ in classifying soil carbon pools, quantifying SOC decomposition kinetics, and representing carbon transfer processes. The structural differences between these two models contributed to the contradictory spatial patterns in simulating SOC storage across the globe (**Figure 2**). Differences in parameter values further cause divergent simulation results between these two models. Parameter values in process-based models quantify the strength, or represent the properties, of different processes in regulating the soil carbon cycle (Luo and Schuur 2020). Previous studies have demonstrated that models sharing the same first-order kinetics for SOC decomposition estimated contrasting soil carbon residence time (Zhou et al. 2018, Wei et al. 2022) and age (He et al. 2016, Shi et al. 2020) due to their different parameterizations. These differences resulted in large uncertainties in simulating global SOC storage (Todd-Brown et al. 2013). While all these simulations are, to some degree, plausible under given assumptions and theories, we need to identify the most probable ones to better understand how the soil carbon cycle responds to a changing climate.

Data assimilation enables converging simulations of global SOC storage by constraining key components in the soil carbon cycle in structurally different process-based models. Regardless of their difference in structure, our results show well-converged global SOC simulations by CLM5 and COMPAS after being optimized by the PRODA approach with the same soil carbon observations. The convergence in SOC simulations derives from the fact that the PRODA approach effectively retrieves the spatial patterns of parameters of

process-based models from observational data. Parameters in CLM5 and COMPAS are both conceptually and functionally different from each other due to their structural dissimilarity (e.g., the turnover time values for conceptually different carbon pools and the carbon transfer coefficients in CLM5 and COMPAS, see Figure 1 and Methods for details). However, the spatial distributions of parameters aggregated into six model components defined in the same way for both models exhibit some agreement between the models. Carbon transfer efficiency, baseline decomposition rate, and environmental modifiers have been identified as determinants in explaining the spatial patterns of global SOC storage by process-based models (Tao et al. 2023b). In this study, these components show converged spatial patterns despite structurally different models after being informed by observations. In contrast, other model components that are less important for determining global SOC storage (e.g., carbon input allocation and vertical transport) did not converge in the simulations by CLM5 and COMPAS. This difference is probably caused by lack of sufficient information in the data to constrain parameters underlying these specific components (more discussion on this issue in Section 4.3).

The converged simulations of SOC and its related components demonstrate the fact that although it is impossible to include all the processes in the soil carbon cycle into one process-based model, unresolved processes can be well accounted for in model parameterization at resolved scales after data assimilation (Luo and Schuur 2020). In this study, COMPAS explicitly describes the microbial CUE that represents the carbon partitioning process in microbial physiology and non-microbial carbon transfer that relates to other biological, chemical and physical reactions driving organic matter transformations in soils. CLM5, however, does not differentiate these two processes in its structure but represents them through aggregated carbon transfer coefficients (see Methods). After being optimized by the PRODA approach, CLM5 simulates similar spatial patterns of the carbon

682 transfer index as COMPAS (**Figure 4**). Similarly, a previous study reported that a process-
683 based model that does not explicitly couple nitrogen-related processes with the soil carbon
684 cycle can still well represent nitrogen limitation after its parameters were constrained by data
685 (Wang et al. 2022).
686
687 **4.2. Data assimilation identifies probable decomposition kinetics at investigated scales**
688 Organic carbon decomposition in soils has been debated for decades. In this study, we
689 compared two possible SOC decomposition kinetics at the global scale, namely a linear first-
690 order kinetic model as represented by CLM5 and a nonlinear Michaelis-Menten kinetic
691 model as represented by COMPAS. Our data assimilation results suggest that first-order
692 kinetics may be the simplest and effective mechanism in explaining global SOC storage and
693 its spatial patterns. After PRODA optimization, CLM5 and COMPAS show similar
694 performance in explaining the spatial variability of SOC across the globe. A linear model
695 such as CLM5 that adequately considers the spatial heterogeneity of its parameters can
696 generate sufficient variability in simulating the soil carbon cycle. Indeed, notwithstanding its
697 simplicity, the linear relationship between the decomposition rate and the substrate
698 concentration has been observed from macroscopic litter and soil organic carbon
699 decomposition experiments (Zhang et al. 2008, Schädel et al. 2014, Xu et al. 2016, Cai et al.
700 2018, Luo 2022).
701 Microorganism-centric kinetics (e.g., Michaelis-Menten kinetics) that considers
702 enzymatic depolymerization has been advocated in recent years to account for the
703 nonlinearity in organic carbon decomposition such that the decomposition rate is a function
704 of both the substrate and the enzyme concentrations. Nonlinear kinetics can help capturing
705 spatial variability of soil carbon dynamics (Wieder et al. 2013) and is necessary for
706 understanding lignin decomposition (Liao et al. 2022) and priming effects (Wutzler and

Reichstein 2008). In this study, our data assimilation results show that, at the global scale, nonlinearity in COMPAS does not necessarily lead to more accurate quantification of SOC storage than CLM5. Moreover, after being informed by data constraints, Michaelis constants in COMPAS were much larger than their corresponding substrate concentrations (**Figure 5**). In such a case, the Michaelis-Menten kinetics can be mathematically approximated by a linear structure with respect to its corresponding substrate, but also including a first order effect of the receiver pool, resulting in a multiplicative kinetics.

It should be noted that diversity in model structures is still necessary for a better understanding of the soil carbon cycle at different spatial and temporal scales. Microbial models with nonlinear structures can be useful for studying complex carbon dynamics at small scales that cannot be explained by linear models (Manzoni and Porporato 2007, Liao et al. 2022). Also the microbial responses to environmental fluctuations are highly nonlinear and can be captured only by modelling specific microbial processes (Brangarí et al. 2020). Moreover, models of SOC storage with different structures can perform differently across subregions, suggesting that some structures are more suitable for certain pedoclimatic conditions. We have observed different patterns of SOC storage simulated by CLM5 and COMPAS in boreal (e.g., East Siberia) and tropical regions (e.g., Amazon and Congo Basins), even though both of the models were constrained by observational SOC data. Moreover, the Michaelis-Menten kinetics investigated in this study is only one possibility from an array of theories. How other nonlinear kinetics (e.g., reverse Michaelis Menten kinetics (Tang and Riley 2019) perform in simulating SOC at different scales in comparison with linear models requires more studies in the future.

4.3 More data required to diminish prediction uncertainty

Uncertainty still exists in predicting SOC storage by structurally different models after PRODA optimization (**Supplementary Figure 2**). The PRODA approach used in this study reveals the spatial heterogeneity of model parameters after site-level data assimilation. Thus, at the global scale, PRODA optimizes about 1.41 million parameter values (21 selected parameters for each of the 66,935 vertical SOC profiles) for CLM5 and 1.37 million parameter values (23 selected parameters for each of the 59,476 vertical SOC profiles) for COMPAS across observational sites. The posterior distributions of different parameters showed substantial uncertainties after data assimilation at site-level. In an example of data assimilation at one site (**Supplementary Figure 2**), while a few parameters can be well constrained by vertical SOC profile data, resulting in narrower posterior distributions than the priors, more than half of the selected parameters had weak identifiability to the observations such that their posterior distribution showed flat shapes within the prior ranges.

The identifiability of different parameters is associated with the convergence of their corresponding model components by structurally different models and further affects the final global SOC simulations (Luo et al. 2009). For parameters that are well constrained by vertical SOC profiles in data assimilation, their corresponding model components (e.g., carbon transfer efficiency, baseline decomposition, and environmental modifiers) also showed similar spatial patterns by CLM5 and COMPAS despite differences in model structures. The revealed spatial patterns of these model components further presented high explanatory power to predict model-simulated SOC spatial patterns across the globe (Tao et al. 2023b). In contrast, for parameters that are less identifiable to observational data in data assimilation, different choices of optimized parameter value could lead to similar simulation results on SOC storage, causing the so-called equifinality problem. Thus, the spatial pattern of their corresponding components, such as vertical transport and carbon input allocation, did

not agree well after data assimilation in different models. Their spatial variability was also less responsible for improved global SOC simulations.

The equifinality problem (or weak identifiability of parameters) imposes challenges to using the optimised models to predict future SOC changes under climate change. In this study, we found that the spatial patterns of vertical transport and carbon input allocation may be less consequential to simulating SOC storage at the steady state at the global scale. However, both these processes can influence the physical disconnection of SOC from decomposers, so they could regulate the transient dynamics of SOC in response to climate change, warranting further investigations. Moreover, despite reasonable correlations between results retrieved from the two structurally different models, carbon transfer efficiency and baseline decomposition simulated by CLM5 and COMPAS are numerically different (i.e., not on the 1:1 line in **Figure 4**). Whether structurally different models after PRODA optimization can also predict converged SOC changes at different temporal scales is still an open question.

Broader inclusion of various kinds of observational data related to soil carbon cycle at different spatial-temporal scales is the key to resolving the equifinality problem and better predictions of SOC dynamics. While this study only used SOC content as the constraint to process-based models, our results clearly demonstrated that applying PRODA approach with observational constraints can effectively realize converged simulations of SOC storage by structurally different models, even if they could generate contrasting simulation results before PRODA optimization.

Beyond SOC content data, an array of measurements could be used in the PRODA approach to further improve model predictive ability and inform model development. First, decomposition data of different soil carbon pools and soil radiocarbon data could help better understand decomposition kinetics. While the decomposition of litter chemical fractions is well characterized, a better understanding of contrasting nutrient limitation mechanisms still

780 needs data beyond time series of litter total carbon, total nitrogen, and lignin (Manzoni et al.
781 2021). Meanwhile, measured carbon pools with clear physical meanings, such as particulate
782 and mineral-associated organic carbon can help to constrain their conceptual counterparts in
783 models (Abramoff et al. 2022, Guo et al. 2022). Second, heterotrophic respiration time series
784 could also be useful in transient conditions, as they vary more than SOC stocks. Third,
785 besides pool and flux data, microbial trait data can inform some of the model parameters, or
786 offer avenues for testing emerging properties such as CUE. For example, data related to
787 microbial carbon use efficiency can potentially constrain carbon transfer related parameters,
788 but only if measurements are representative of in situ conditions (e.g., using the ^{18}O
789 incorporation method instead of adding labile ^{13}C sources) (Geyer et al. 2019). Moreover,
790 including observations related to vegetation and hydrology dynamics in data assimilation
791 may be more effective in understanding the spatial patterns of carbon input allocation and
792 vertical transport.
793
794

5. Conclusion

This study highlights the importance of data in constraining model development and simulations. While diverse model structures and varying parameterizations generate an array of possibilities in simulating SOC storage under different assumptions and theories, data assimilation identifies the most probable ones that best explain the observations. The PRODA approach in this study optimizes the parameters of a model based on first-order kinetics (i.e., CLM5) and one based on Michaelis-Menten kinetics (i.e., COMPAS). Optimised parameters lead to convergence in simulated SOC storage and its related key components (i.e., the main contributing mechanisms), such as carbon transfer and baseline decomposition. Meanwhile, our PRODA approach identifies the first-order kinetics as an equally effective explanation with the Michaelis-Menten kinetics for global SOC storage. In the future, it is still critical to explore various processes of the soil carbon cycle at different scales by developing structurally different models to be tested with new data sets. A tool such as PRODA will be critical in reconciling field observations and theoretical reasoning in modelling. New findings and patterns revealed by the PRODA approach will further stimulate new data acquisition and improvement of models.

References

Abramoff, R. Z., B. Guenet, H. Zhang, K. Georgiou, X. Xu, R. A. V. Rossel, W. Yuan, and P. Ciais. 2022. Improved global-scale predictions of soil carbon stocks with Millennial Version 2. Soil Biology and Biochemistry **164**:108466.

Allison, S. D., M. D. Wallenstein, and M. A. Bradford. 2010. Soil-carbon response to warming dependent on microbial physiology. Nature Geoscience **3**:336-340.

Batjes, N. H., E. Ribeiro, and A. Van Oostrum. 2020. Standardised soil profile data to support global mapping and modelling (WoSIS snapshot 2019). Earth System Science Data **12**:299-320.

Beck, H. E., N. E. Zimmermann, T. R. McVicar, N. Vergopolan, A. Berg, and E. F. Wood. 2018. Present and future Köppen-Geiger climate classification maps at 1-km resolution. Scientific data **5**:180214.

Bradford, M. A., W. R. Wieder, G. B. Bonan, N. Fierer, P. A. Raymond, and T. W. Crowther. 2016. Managing uncertainty in soil carbon feedbacks to climate change. Nature Climate Change **6**:751-758.

Brangarí, A. C., S. Manzoni, and J. Rousk. 2020. A soil microbial model to analyze decoupled microbial growth and respiration during soil drying and rewetting. Soil Biology and Biochemistry **148**:107871.

Cai, A., G. Liang, X. Zhang, W. Zhang, L. Li, Y. Rui, M. Xu, and Y. Luo. 2018. Long-term straw decomposition in agro-ecosystems described by a unified three-exponentiation equation with thermal time. Science of the Total Environment **636**:699-708.

Chandel, A., L. Jiang, and Y. Luo. 2023. Microbial Models for Simulating Soil Carbon Dynamics: A Review. Journal of Geophysical Research - Biogeosciences.

Ciais, P., C. Sabine, G. Bala, L. Bopp, V. Brovkin, J. Canadell, A. Chhabra, R. DeFries, J. Galloway, M. Heimann, C. Jones, C. L. Quéré, R. Myneni, S. Piao, P. Thornton, N. Metzl, and R. Wania. 2014. Carbon and other biogeochemical cycles. Pages 465-570 Climate change 2013: the physical science basis. Contribution of Working Group I to the Fifth Assessment Report of the Intergovernmental Panel on Climate Change. Cambridge University Press.

Cotrufo, M. F., J. L. Soong, A. J. Horton, E. E. Campbell, M. L. Haddix, D. H. Wall, and W. J. Parton. 2015. Formation of soil organic matter via biochemical and physical pathways of litter mass loss. Nature Geoscience **8**:776-779.

Cotrufo, M. F., M. D. Wallenstein, C. M. Boot, K. Denef, and E. Paul. 2013. The Microbial Efficiency-Matrix Stabilization (MEMS) framework integrates plant litter decomposition with soil organic matter stabilization: do labile plant inputs form stable soil organic matter? Global change biology **19**:988-995.

Fick, S. E., and R. J. Hijmans. 2017. WorldClim 2: new 1-km spatial resolution climate surfaces for global land areas. International Journal of Climatology **37**:4302-4315.

Forney, D. C., and D. H. Rothman. 2012. Common structure in the heterogeneity of plant-matter decay. Journal of The Royal Society Interface **9**:2255-2267.

Gelman, A., J. B. Carlin, H. S. Stern, D. B. Dunson, A. Vehtari, and D. B. Rubin. 2014. Bayesian data analysis. CRC press Boca Raton, FL.

Georgiou, K., R. Z. Abramoff, J. Harte, W. J. Riley, and M. S. Torn. 2017. Microbial community-level regulation explains soil carbon responses to long-term litter manipulations. Nature communications **8**:1-10.

Geyer, K. M., P. Dijkstra, R. Sinsabaugh, and S. D. Frey. 2019. Clarifying the interpretation of carbon use efficiency in soil through methods comparison. Soil Biology and Biochemistry **128**:79-88.

Geyer, K. M., E. Kyker-Snowman, A. S. Grandy, and S. D. Frey. 2016. Microbial carbon use efficiency: accounting for population, community, and ecosystem-scale controls over the fate of metabolized organic matter. Biogeochemistry **127**:173-188.

Grigal, D., S. Brovold, W. Nord, and L. Ohmann. 1989. Bulk density of surface soils and peat in the north central United States. Canadian Journal of Soil Science **69**:895-900.

Guo, X., R. A. Viscarra Rossel, G. Wang, L. Xiao, M. Wang, S. Zhang, and Z. Luo. 2022. Particulate and mineral-associated organic carbon turnover revealed by modelling their long-term dynamics. Soil Biology and Biochemistry **173**:108780.

Haario, H., E. Saksman, and J. Tamminen. 2001. An adaptive Metropolis algorithm. Bernoulli **7**:223-242.

He, X., R. Abramoff, E. Abs, K. Georgiou, H. Zhang, and D. S. Goll. 2023. Contribution of carbon inputs to soil carbon accumulation cannot be neglected. bioRxiv:2023.2007. 2017.549330.

He, Y., S. E. Trumbore, M. S. Torn, J. W. Harden, L. J. Vaughn, S. D. Allison, and J. T. Randerson. 2016. Radiocarbon constraints imply reduced carbon uptake by soils during the 21st century. science **353**:1419-1424.

Hengl, T., J. M. de Jesus, G. B. Heuvelink, M. R. Gonzalez, M. Kilibarda, A. Blagotić, W. Shangguan, M. N. Wright, X. Geng, and B. Bauer-Marschallinger. 2017. SoilGrids250m: Global gridded soil information based on machine learning. PLoS One **12**:e0169748.

Huang, Y., X. Lu, Z. Shi, D. Lawrence, C. D. Koven, J. Xia, Z. Du, E. Kluzek, and Y. Luo. 2018. Matrix approach to land carbon cycle modeling: A case study with the Community Land Model. Global change biology **24**:1394-1404.

Hugelius, G., C. Tarnocai, G. Broll, J. Canadell, P. Kuhry, and D. Swanson. 2013. The Northern Circumpolar Soil Carbon Database: spatially distributed datasets of soil coverage and soil carbon storage in the northern permafrost regions. Earth System Science Data **5**:3-13.

Jackson, R., J. Canadell, J. R. Ehleringer, H. Mooney, O. Sala, and E. Schulze. 1996. A global analysis of root distributions for terrestrial biomes. Oecologia **108**:389-411.

Jackson, R. B., K. Lajtha, S. E. Crow, G. Hugelius, M. G. Kramer, and G. Piñeiro. 2017. The ecology of soil carbon: pools, vulnerabilities, and biotic and abiotic controls. Annual Review of Ecology, Evolution, and Systematics **48**:419-445.

Janssen, P., and P. Heuberger. 1995. Calibration of process-oriented models. Ecological modelling **83**:55-66.

Lasaga, A. C. 1998. Kinetic theory in the earth sciences. Princeton university press.

Lawrence, D., R. Fisher, C. Koven, K. Oleson, S. Swenson, M. Vertenstein, B. Andre, G. Bonan, B. Ghimire, L. van Kampenhout, D. Kennedy, E. Kluzek, R. Knox, P. Lawrence, F. Li, H. Li, D. Lombardozzi, Y. Lu, J. Perket, W. Riley, W. Sacks, M. Shi, W. Wieder, C. Xu, A. Ali, A. Badger, G. Bisht, P. Broxton, M. Brunke, J. Buzan, M. Clark, T. Craig, K. Dahlin, B. Drewniak, L. Emmons, J. Fisher, M. Flanner, P. Gentine, J. Lenaerts, S. Levis, L. R. Leung, W. Lipscomb, J. Pelletier, D. M. Ricciuto, B. Sanderson, J. Shuman, A. Slater, Z. Subin, J. Tang, A. Tawfik, Q. Thomas, S. Tilmes, F. Vitt, and X. Zeng. 2018. Technical Description of version 5.0 of the Community Land Model (CLM).

Lawrence, D. M., R. A. Fisher, C. D. Koven, K. W. Oleson, S. C. Swenson, G. Bonan, N. Collier, B. Ghimire, L. van Kampenhout, and D. Kennedy. 2019. The Community

907 Land Model version 5: Description of new features, benchmarking, and impact of
908 forcing uncertainty. Journal of Advances in Modeling Earth Systems **11**:4245-4287.
909 Li, Q., J. Xia, Z. Shi, K. Huang, Z. Du, G. Lin, and Y. Luo. 2016. Variation of parameters in a
910 Flux-Based Ecosystem Model across 12 sites of terrestrial ecosystems in the
911 conterminous USA. Ecological modelling **336**:57-69.
912 Liao, C., X. Lu, Y. Huang, D. Lawrence, E. Kluzek, K. Oleson, W. Wieder, and Y. Luo. 2022.
913 Accelerated spin-up of Community Land Model version 5 (CLM5) with coupled
914 terrestrial carbon and nitrogen cycles. in prep.
915 Lu, X., Z. Du, Y. Huang, D. Lawrence, E. Kluzek, N. Collier, D. Lombardozzi, N. Sobhani,
916 E. A. Schuur, and Y. Luo. 2020. Full Implementation of Matrix Approach to
917 Biogeochemistry Module of CLM5. Journal of Advances in Modeling Earth Systems
918 **12**:e2020MS002105.
919 Lu, X., Y.-P. Wang, Y. Luo, and L. Jiang. 2018. Ecosystem carbon transit versus turnover
920 times in response to climate warming and rising atmospheric CO 2 concentration.
921 Biogeosciences **15**:6559-6572.
922 Luo, Y. 2022. Theoretical foundation of the land carbon cycle and matrix approach. Land
923 Carbon Cycle Modeling: Matrix Approach, Data Assimilation, & Ecological
924 Forecasting. CPC Press, Taylor & Francis Group, Boca Raton, Florida.
925 Luo, Y., A. Ahlström, S. D. Allison, N. H. Batjes, V. Brovkin, N. Carvalhais, A. Chappell, P.
926 Ciais, E. A. Davidson, and A. Finzi. 2016. Toward more realistic projections of soil
927 carbon dynamics by Earth system models. Global biogeochemical cycles **30**:40-56.
928 Luo, Y., Y. Huang, C. A. Sierra, J. Xia, A. Ahlström, Y. Chen, O. Hararuk, E. Hou, L. Jiang,
929 C. Liao, X. Lu, Z. Shi, B. Smith, F. Tao, and Y.-P. Wang. 2022. Matrix approach to
930 land carbon cycle modeling. Journal of Advances in Modeling Earth
931 Systems:e2022MS003008.
932 Luo, Y., T. F. Keenan, and M. Smith. 2015. Predictability of the terrestrial carbon cycle.
933 Global change biology **21**:1737-1751.
934 Luo, Y., K. Ogle, C. Tucker, S. Fei, C. Gao, S. LaDeau, J. S. Clark, and D. S. Schimel. 2011.
935 Ecological forecasting and data assimilation in a data-rich era. Ecological
936 Applications **21**:1429-1442.
937 Luo, Y., and E. A. Schuur. 2020. Model parameterization to represent processes at unresolved
938 scales and changing properties of evolving systems. Global change biology **26**:1109-
939 1117.
940 Luo, Y., E. Weng, X. Wu, C. Gao, X. Zhou, and L. Zhang. 2009. Parameter identifiability,
941 constraint, and equifinality in data assimilation with ecosystem models. Ecological
942 Applications **19**:571-574.
943 Manzoni, S., P. Čapek, P. Porada, M. Thurner, M. Winterdahl, C. Beer, V. Brüchert, J. Frouz,
944 A. M. Herrmann, and B. D. Lindahl. 2018. Reviews and syntheses: Carbon use
945 efficiency from organisms to ecosystems–definitions, theories, and empirical
946 evidence. Biogeosciences **15**:5929-5949.
947 Manzoni, S., A. Chakrawal, M. Spohn, and B. D. Lindahl. 2021. Modeling microbial
948 adaptations to nutrient limitation during litter decomposition. Frontiers in Forests and
949 Global Change **4**:686945.
950 Manzoni, S., and A. Porporato. 2007. A theoretical analysis of nonlinearities and feedbacks in
951 soil carbon and nitrogen cycles. Soil Biology and Biochemistry **39**:1542-1556.
952 Mishra, U., S. Gautam, W. Riley, and F. M. Hoffman. 2020. Ensemble machine learning
953 approach improves predicted spatial variation of surface soil organic carbon stocks in
954 data-limited northern circumpolar region. Frontiers in Big Data **3**:40.

Parton, W., D. S. Schimel, C. Cole, and D. Ojima. 1987. Analysis of factors controlling soil organic matter levels in great plains grasslands1. Soil science society of America journal **51**:1173-1179.

Parton, W. J., J. W. Stewart, and C. V. Cole. 1988. Dynamics of C, N, P and S in grassland soils: a model. Biogeochemistry **5**:109-131.

Schädel, C., E. A. Schuur, R. Bracho, B. Elberling, C. Knoblauch, H. Lee, Y. Luo, G. R. Shaver, and M. R. Turetsky. 2014. Circumpolar assessment of permafrost C quality and its vulnerability over time using long-term incubation data. Global change biology **20**:641-652.

Schimel, J. P., and M. N. Weintraub. 2003. The implications of exoenzyme activity on microbial carbon and nitrogen limitation in soil: a theoretical model. Soil Biology and Biochemistry **35**:549-563.

Schmidt, M. W., M. S. Torn, S. Abiven, T. Dittmar, G. Guggenberger, I. A. Janssens, M. Kleber, I. Kögel-Knabner, J. Lehmann, and D. A. Manning. 2011. Persistence of soil organic matter as an ecosystem property. Nature **478**:49.

Shi, Z., S. D. Allison, Y. He, P. A. Levine, A. M. Hoyt, J. Beem-Miller, Q. Zhu, W. R. Wieder, S. Trumbore, and J. T. Randerson. 2020. The age distribution of global soil carbon inferred from radiocarbon measurements. Nature Geoscience **13**:555-559.

Tang, J., and W. J. Riley. 2019. Competitor and substrate sizes and diffusion together define enzymatic depolymerization and microbial substrate uptake rates. Soil Biology and Biochemistry **139**:107624.

Tao, F., B. Z. Houlton, S. D. Frey, J. Lehmann, S. Manzoni, Y. Huang, L. Jiang, U. Mishra, B. A. Hungate, and M. W. Schmidt. 2023a. Reply to: Contribution of carbon inputs to soil carbon accumulation cannot be neglected. bioRxiv:2023.2008. 2020.552557.

Tao, F., Y. Huang, B. A. Hungate, S. Manzoni, S. D. Frey, M. W. I. Schmidt, M. Reichstein, N. Carvalhais, P. Ciais, L. Jiang, J. Lehmann, Y.-P. Wang, B. Z. Houlton, B. Ahrens, U. Mishra, G. Hugelius, T. D. Hocking, X. Lu, Z. Shi, K. Viatkin, R. Vargas, Y. Yigini, C. Omuto, A. A. Malik, G. Peralta, R. Cuevas-Corona, L. E. Di Paolo, I. Luotto, C. Liao, Y.-S. Liang, V. S. Saynes, X. Huang, and Y. Luo. 2023b. Microbial carbon use efficiency promotes global soil carbon storage. Nature **618**:981-985.

Tao, F., and Y. Luo. 2022. PROcess-guided deep learning and DAta-driven modelling (PRODA).*in* Y. Luo and B. Smith, editors. Land Carbon Cycle Modeling: Matrix Approach, Data Assimilation, and Ecological Forecasting. Taylor and Francis.

Tao, F., Z. Zhou, Y. Huang, Q. Li, X. Lu, S. Ma, X. Huang, Y. Liang, G. Hugelius, L. Jiang, R. Doughty, Z. Ren, and Y. Luo. 2020. Deep Learning Optimizes Data-Driven Representation of Soil Organic Carbon in Earth System Model Over the Conterminous United States. Frontiers in Big Data **3**.

Todd-Brown, K., J. Randerson, W. Post, F. Hoffman, C. Tarnocai, E. Schuur, and S. Allison. 2013. Causes of variation in soil carbon simulations from CMIP5 Earth system models and comparison with observations. Biogeosciences **10**:1717-1736.

Wang, S., Y. Luo, and S. Niu. 2022. Reparameterization Required After Model Structure Changes From Carbon Only to Carbon-Nitrogen Coupling. Journal of Advances in Modeling Earth Systems **14**:e2021MS002798.

Wang, Y. p., H. Zhang, P. Ciais, D. Goll, Y. Huang, J. D. Wood, S. V. Ollinger, X. Tang, and A. k. Prescher. 2021. Microbial activity and root carbon inputs are more important than soil carbon diffusion in simulating soil carbon profiles. Journal of Geophysical Research: Biogeosciences **126**:e2020JG006205.

Wei, N., J. Xia, J. Zhou, L. Jiang, E. Cui, J. Ping, and Y. Luo. 2022. Evolution of uncertainty in terrestrial carbon storage in earth system models from CMIP5 to CMIP6. Journal of Climate **35**:5483-5499.

Wieder, W. R., G. B. Bonan, and S. D. Allison. 2013. Global soil carbon projections are improved by modelling microbial processes. Nature Climate Change **3**:909-912.

Wilson, C. H., and S. Gerber. 2021. Theoretical insights from upscaling Michaelis–Menten microbial dynamics in biogeochemical models: a dimensionless approach. Biogeosciences **18**:5669-5679.

Wutzler, T., and M. Reichstein. 2008. Colimitation of decomposition by substrate and decomposers–a comparison of model formulations. Biogeosciences **5**:749-759.

Xu, T., L. White, D. Hui, and Y. Luo. 2006. Probabilistic inversion of a terrestrial ecosystem model: Analysis of uncertainty in parameter estimation and model prediction. Global biogeochemical cycles **20**.

Xu, X., Z. Shi, D. Li, A. Rey, H. Ruan, J. M. Craine, J. Liang, J. Zhou, and Y. Luo. 2016. Soil properties control decomposition of soil organic carbon: Results from data-assimilation analysis. Geoderma **262**:235-242.

Yigini, Y., G. Olmedo, S. Reiter, R. Baritz, K. Viatkin, and R. Vargas. 2018. Soil organic carbon mapping: cookbook.

Zhang, D., D. Hui, Y. Luo, and G. Zhou. 2008. Rates of litter decomposition in terrestrial ecosystems: global patterns and controlling factors. Journal of Plant Ecology **1**:85-93.

Zhou, S., J. Liang, X. Lu, Q. Li, L. Jiang, Y. Zhang, C. R. Schwalm, J. B. Fisher, J. Tjiputra, and S. Sitch. 2018. Sources of uncertainty in modeled land carbon storage within and across three MIPs: Diagnosis with three new techniques. Journal of Climate **31**:2833-2851.

Zhou, T., P. Shi, G. Jia, Y. Dai, X. Zhao, W. Shangguan, L. Du, H. Wu, and Y. Luo. 2015. Age-dependent forest carbon sink: Estimation via inverse modeling. Journal of Geophysical Research: Biogeosciences **120**:2473-2492.

Zhou, T., P. Shi, G. Jia, and Y. Luo. 2013. Nonsteady state carbon sequestration in forest ecosystems of China estimated by data assimilation. Journal of Geophysical Research: Biogeosciences **118**:1369-1384.

Acknowledgement:

F.T. is supported by the Eric and Wendy Schmidt AI in Science Postdoctoral Fellowship, a Schmidt Futures program. S.M. has received funding from the European Research Council (ERC) under the European Union's Horizon 2020 Research and Innovation Programme (grant agreement no 101001608).

Supplementary Tables and Figures

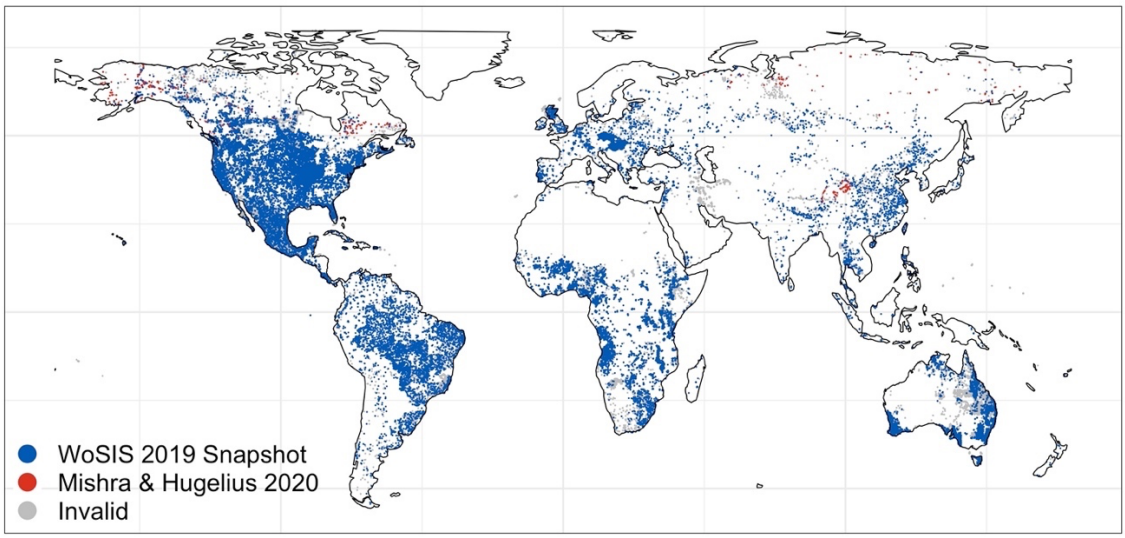

Supplementary Figure 1. Geographic distributions of vertical SOC profiles used in this study.

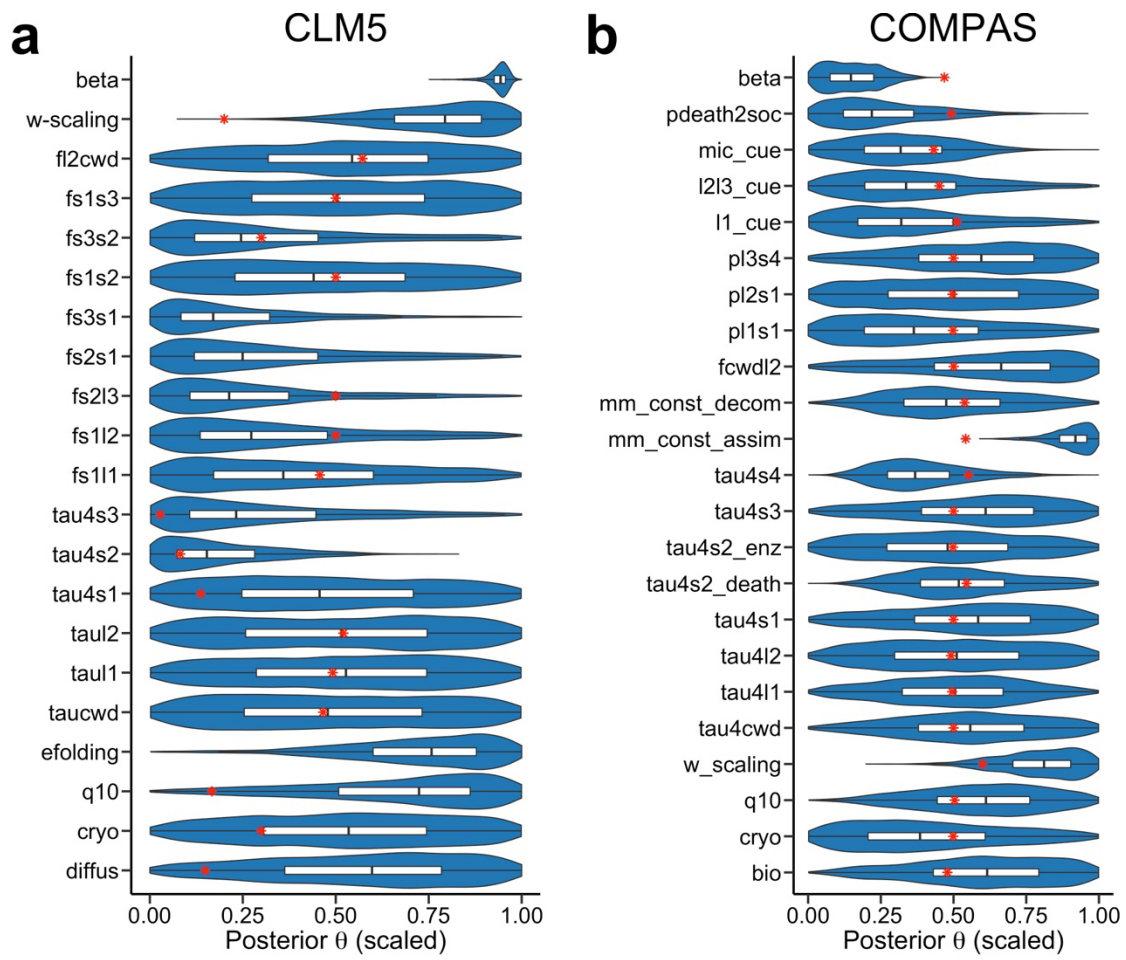

Supplementary Figure 2. Posterior distributions of parameters after data assimilation at one site (98.27W, 55.90N) using CLM5 (a) and COMPAS (b). Violin plots present the shapes of posterior distributions. The lower, middle, and upper hinges of boxplots show the first, median, and third quartiles of the distribution. Whiskers in the boxplot represent the 1.5 times the interquartile range from the hinges. Red stars indicate the default (ad hoc) parameter values used in global simulations. Parameter values are scaled by their prior ranges (**Supplementary Tables 1 - 2**). Note that for parameters that are set to vary across space in the original CLM5, there is an absence of red stars. Moreover, default CLM5 set the default efolding value as 10. In this study, we set the prior range of efolding as [0, 1]. Thus, the default value of efolding in CLM5 is not shown in panel a.

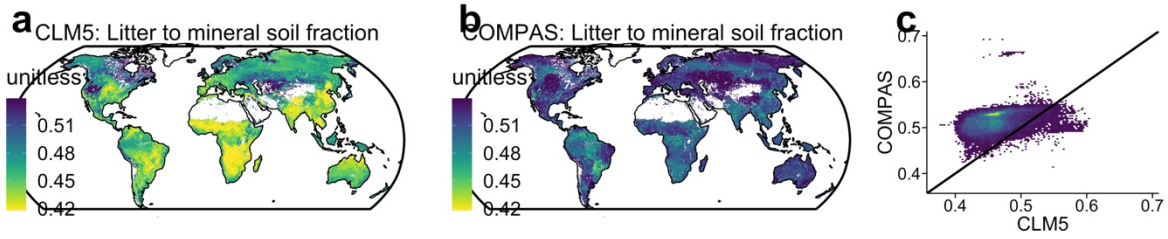

Supplementary Figure 3. Spatial patterns of the ratio of litter carbon transferred to mineral soil over the total carbon input, as simulated by (a) CLM5 and (b) COMPAS after PRODA optimization. (c) Comparison of the same ratio as simulated by the two models.

Supplementary Table 1 | Parameters in CLM5 that were optimized in the profile-level data assimilation.

No.	Name	Matrix term	Corresponding mechanism	Description	Default values	Unit	Prior range in profile-level data assimilation
1	*fs3s1*	**A**	Microbial carbon use efficiency (CUE)	Transfer fraction, fast SOC to passive SOC	Sand dependent	unitless	[0 0.05]
2	*fs3s2*	**A**		Transfer fraction, slow SOC to passive SOC	0.03	unitless	[0 0.1]
3	*fs2s1*	**A**		Transfer fraction, fast SOC to slow SOC	Sand dependent	unitless	[0 0.4]
4	*fs2l3*	**A**		Transfer fraction, lignin litter to slow SOC	0.5	unitless	[0.2 0.8]
5	*fs1l2*	**A**		Transfer fraction, cellulose litter to fast SOC	0.5	unitless	[0.2 0.8]
6	*fs1l1*	**A**		Transfer fraction, metabolic litter to fast SOC	0.45	unitless	[0.1 0.8]
7	*fs1s2*	**A**		Transfer fraction, slow SOC to fast SOC	0.42	unitless	[0.1 0.74]
8	*fs1s3*	**A**		Transfer fraction, passive SOC to fast SOC	0.45	unitless	[0 0.9]
9	*fl2cwd*	**A**		Transfer fraction, coarse woody debris to cellulose litter	0.786	unitless	[0.5 1]
10	*tau4s2*	**K**	Substrate decomposability	Turnover time of slow SOC	5	year	[1 50]
11	*tau4s3*	**K**		Turnover time of passive SOC	222.222	year	[200 1000]
12	*tau4s1*	**K**		Turnover time of fast SOC	0.1370	year	[0 1]
13	*tau4l1*	**K**		Turnover time of metabolic litter	0.0541	year	[0 0.11]
14	*tau4cwd*	**K**		Turnover time of coarse woody debris	3.33	year	[1 6]
15	*tau4l2*	**K**		Turnover time of cellulose and lignin litter	0.2041	year	[0.1 0.3]
16	*w-scaling*	**ξ**	Environmental modifiers	Scaling factor to soil water scalar	1	unitless	[0 5]
17	*q10*	**ξ**		Temperature sensitivity	1.5	unitless	[1.2 3]
18	*efolding*	**ξ**		E-folding parameter to calculate depth scalar	10	metre	[0, 1]
19	*cryo*	**V**	Vertical transport	Cryoturbation rate	0.0005	m^2yr^{-1}	$[3\times10^{-5}\ 16\times10^{-4}]$
20	*diffus*	**V**		Bioturbation rate	0.0001	m^2yr^{-1}	$[3\times10^{-5}\ 5\times10^{-4}]$
21	*b*	**I**	Carbon input allocation	Parameter controlling vertical distribution of carbon input to litter pools	PFT dependent	unitless	[0.5 1]

Supplementary Table 2 | Parameters in COMPAS that were optimized in the profile-level data assimilation.

No.	Name	Related components	Description	Default values	Unit	Prior range
1	η_{DOC}	Microbial carbon use efficiency	Microbial CUE for DOC assimilation	0.27	unitless	[0.01 0.7]
2	η_{ML}		Microbial CUE for metabolic litter assimilation	0.66	unitless	[0.4, 0.9]
3	η_{CL-LL}		Microbial CUE for cellulose/lignin litter assimilation	0.16	unitless	[0, 0.4]
4	$K_{m,assim}$		Concentration of DOC for half max DOC assimilation reaction	1.8×10^{3}	gCm^{-3}	[300 3000]
5	τ_{assim}		Inverse of $v_{max,assim}$ in DOC assimilation	0.015	year	[0.03 0.001]
6	τ_{decom}	Decomposition	Inverse of $v_{max,decom}$ in SOC decomposition	1.62×10^{-4}	year	$[0\ 3\times10^{-4}]$
7	$K_{m,decom}$		Concentration of SOC for half max SOC decomposition reaction	5.65×10^{5}	gCm^{-3}	$[10^{5}\ 10^{6}]$
8	$\tau_{ENZ,prod}$		Turnover time for enzyme production	22	year	[15 30]
9	τ_{ML}		Turnover time of metabolic litter	0.049	year	[0 0.1]
10	τ_{CWD}		Turnover time of coarse woody debris	3.5	year	[1 6]
11	τ_{CL-LL}		Turnover time of cellulose and lignin litter	0.2	year	[0.1 0.3]
12	$\tau_{ENZ,decay}$		Turnover time for enzyme decay	0.04	year	[0.001 1]
13	τ_{MIC}		Turnover time for microbial mortality	1.1	year	[0 2]
14	$a_{SOC,MIC}$	Carbon transfer fraction	Fraction of microbial necromass that is stabilized as SOC	0.47	year	[0 1]
15	$a_{CL,CWD}$		Fraction of decomposed CWD that goes to cellulose litter	0.75	unitless	[0.5, 1]
16	$a_{DOC,ML}$		Fraction of total decomposed metabolic litter that goes to DOC	0.05	unitless	[0 0.1]
17	$a_{DOC,CL}$		Fraction of total decomposed cellulose litter that goes to DOC	0.17	unitless	[0.05 0.3]
18	$a_{SOC,LL}$		Fraction of total decomposed lignin litter that goes to SOC	0.78	unitless	[0.6 0.95]
19	*w-scaling*	Environmental modification	Scaling factor to soil water scalar	2.9	unitless	[0 5]
20	*q10*		Temperature sensitivity	2.1	unitless	[1.2 3]
21	*cryo*	Vertical transport	Cryoturbation rate	0.0008	$m^{2}yr^{-1}$	$[3\times10^{-5}\ 16\times10^{-4}]$
22	*diffus*		Bioturbation rate	0.00026	$m^{2}yr^{-1}$	$[3\times10^{-5}\ 5\times10^{-4}]$
23	*b*	Carbon input allocation	Parameter controlling vertical distribution of carbon input to litter pools	0.72	unitless	[0.5 1]

Supplementary Table 3 | Forcing variables for driving simulations of SOC by process-based models.

Variable Names	Full Description	Resolution
nbedrock	Soil layer number that reaches the bedrock	0.5 degree, monthly record of 20-year simulation after the system reaches the steady state.
ALTMAX	Maximum active layer depth of current year	
ALTMAX_LASTYEAR	Maximum active layer depth of last year	
CELLSAND	Sand content	
NPP	Net primary productivity	
SOILPSI	Soil water potential	
TSOI	Soil temperature	
O_SCALAR	Oxygen scalar for decomposition	
FPI_vr	Nitrogen scalar for decomposition	

These forcing variables were the outputs from CLM5 simulation.

Supplementary Table 4 | Environmental variables used in predicting optimized parameter values of process-based models by the deep learning model. Note that information of some of the variables (e.g., clay content) was reported at different depths (i.e., 0cm, 30cm, and 100cm).

No.	Variable Name	Data Source	Category	Description
1	Longitude	WoSIS		
2	Latitude	WoSIS		
3	Elevation	NOAA	Geography	Available at https://www.ngdc.noaa.gov/mgg/global/
4	Absolute Depth to Bedrock	(Hengl et al. 2017)		
5	Bedrock Depth	CLM5 simulation		
6	Koppen Climate Classification	(Beck et al. 2018)		
7	Annual Mean Temperature			
8	Mean Diurnal Range Temperature			
9	Isothermality			
10	Temperature Seasonality			
11	Max Temperature of Warmest Month			
12	Min Temperature of Coldest Month			
13	Temperature Annual Range			
14	Mean Temperature of Wettest Quarter			
15	Mean Temperature of Driest Quarter			
16	Mean Temperature of Warmest Quarter	(Fick and Hijmans 2017)	Climate	
17	Mean Temperature of Coldest Quarter			
18	Annual Precipitation			
19	Precipitation of Wettest Month			
20	Precipitation of Driest Month			
21	Precipitation Seasonality			
22	Precipitation of Wettest Quarter			
23	Precipitation of Driest Quarter			
24	Precipitation of Warmest Quarter			
25	Precipitation of Coldest Quarter			
26	USDA 2014 Suborder Classes			
27	WRB 2006 Subgroup Classes			
28	Coarse Fragments Volumetric			Three depths were included, which are 0cm, 30cm and 100cm, respectively
29	Clay Content	(Hengl et al. 2017)	Soil Texture	Three depths were included, which are 0cm, 30cm and 100cm, respectively
30	Silt Content			Three depths were included, which are 0cm, 30cm and 100cm, respectively
31	Texture Classes			Three depths were included, which are 0cm, 30cm and 100cm, respectively
32	Sand Content			Three depths were included, which are 0cm, 30cm and 100cm, respectively
33	Bulk Density			Three depths were included, which are 0cm, 30cm and 100cm, respectively
34	Soil Water Capacity			Three depths were included, which are 0cm, 30cm and 100cm, respectively
35	Soil pH in H_2O			Three depths were included, which are 0cm, 30cm and 100cm, respectively
36	Soil pH	(Hengl et al. 2017)	Soil Chemical Properties	Three depths were included, which are 0cm, 30cm and 100cm, respectively
37	Cation Exchange Capacity			Three depths were included, which are 0cm, 30cm and 100cm, respectively
38	Grade of a Sub-Soil Being Acid			
39	ESA Land Cover	ESA. Land Cover CCI Product User	Vegetation	Available at: maps.elie.ucl.ac.be/CCI/viewer/download/ESACCI-LC-Ph2-PUGv2_2.0.pdf

		Guide Version 2. Tech. Rep. (2017).	
40	NPP	CLM5 simulation	Mean value of 20-year simulation after the system reaches the steady state
41	Standard deviation of NPP		Standard deviation of 20-year simulation after the system reaches the steady state
42	Vegetation Carbon Stock		Mean value of 20-year simulation after the system reaches the steady state

1084

1085

1086